Overcoming subsurface challenges in the Denise gas field (offshore Nile Delta): an integrated acoustic impedance and machine learning approach for reservoir characterization

Adel Mahmoud Negm[1] · Mohamed I. Abdel-Fattah[2,3] · Dhyaa H. Haddad[4] · Mohamed Reda[1,5] · Ahmed I. Albrkawy[3,6] · Mansour H. Al-Hashim[7]

[1] Geology Department, Faculty of Science, Al-Azhar University, Cairo 11884, Egypt

[2] Petroleum Geosciences and Remote Sensing Program, Department of Applied Physics and Astronomy, College of Sciences, University of Sharjah, 27272 Sharjah, UAE

[3] Geology Department, Faculty of Science, Suez Canal University, Ismailia, Egypt

[4] Petroleum Engineering Department, College of Engineering, Al-Farqadein University, Basrah 61014, Iraq

[5] Department of Petroleum Engineering, College of Engineering, Almaaqal University, Basrah 61014, Iraq

[6] 3D Seismic Lab, School of Earth and Environmental Sciences, Cardiff University, Main Building, Park Place, Cardiff CF10 3AT, UK

[7] Department of Geology and Geophysics, College of Science, King Saud University, Riyadh 11451, Saudi Arabia

Abstract
Reliable reservoir characterization in the offshore Nile Delta is often hindered by intricate channelized depositional architectures, pronounced lateral facies variability, and inconsistent seismic data quality. This study introduces an integrated workflow that combines post-stack acoustic impedance (AI) inversion with probabilistic neural network (PNN) modelling to improve reservoir assessment in the Denise Field, offshore the Nile Delta. The model-based post-stack inversion produced a high-resolution AI volume that exhibits strong agreement (> 90%) with impedance derived from well logs and effectively distinguishes the upper and lower channel systems as low-impedance anomalies indicative of gas-bearing sands. To extend reservoir property prediction beyond well control, a PNN was trained using stepwise-optimized seismic attributes to predict clay volume (V_{cl}), effective porosity (ϕ), and water saturation (S_w). The PNN predictions exhibit excellent agreement with well-log data, with average correlation coefficients of ~ 0.98 for V_{cl} and porosity and ~ 0.87 for water saturation. The resulting 3D property volumes reveal pronounced reservoir heterogeneity and identify laterally continuous channel cores with low shale content, high porosity, and low water saturation. High-quality reservoir zones are concentrated primarily in the western segment of the upper channel, where porosity locally exceeds 25%, and water saturation is generally below 30%. Integrated interpretation of AI, porosity, and saturation volumes confirm strong consistency between elastic and petrophysical indicators, providing independent validation of gas-charged sands and improved confidence in reservoir connectivity. The combined inversion–PNN workflow significantly reduces interpretation uncertainty, enhances predictions of reservoir properties in areas with sparse well control, and provides a robust basis for identifying producible hydrocarbon zones. These findings highlight the value of combining seismic inversion with machine-learning approaches to improve reservoir characterization and support development planning in the offshore Nile Delta and in comparable clastic gas systems worldwide.

Keywords Seismic attributes; Probabilistic neural network (PNN); Model-based inversion; Reservoir characterization; Offshore Nile Delta; Denise field

1 Introduction

The offshore Nile Delta represents one of the most prolific gas provinces in the Mediterranean region, hosting numerous Miocene to Pleistocene clastic reservoirs characterized by rapid sedimentation, strong lateral facies variability, and complex post-depositional structural modification (Abdel-Fattah et al. 2022; Shehata et al. 2023; Fathy et al. 2025a, b; Reda et al. 2025c; Raef et al. 2025). Within this province, the Denise gas field, located in the eastern offshore Nile Delta, constitutes a mature producing asset. However, its subsurface characterization remains challenging due to the combined effects of heterogeneous depositional systems, salt-related tectonics, and variable seismic data quality (Abdel-Fattah and Slatt 2013; Negm et al. 2025). These factors collectively obscure reservoir geometry and complicate the reliable prediction of lithology, petrophysical properties, and fluid distribution, even in well-developed fields.

The Denise Field lies approximately 7 km north of the Mediterranean shoreline of Egypt in water depths of about 70–75 m and covers an area of nearly 400 km² (Fig. 1). Discovered in 1977 and brought on production in 1999, the field produces gas and condensates from channelized clastic reservoirs within the Neogene succession. Regionally, the Nile Delta Basin is estimated to contain several trillion cubic feet of recoverable gas, emphasizing the continued importance of improving reservoir characterization workflows to maximize recovery and reduce development risk (Badalini et al. 2020; Abdel-Rahman et al. 2025). In the Denise area, reservoirs are typically associated with stacked fluvial–deltaic and shallow-marine channel sands that are encased within shale-prone successions, resulting in strong heterogeneity and potential compartmentalization (Othman et al. 2018; Fathy et al. 2026; Abdel-Fattah et al. 2023).

A key challenge in the Denise Field is discriminating against gas-bearing sand bodies from surrounding shale and water-saturated facies using seismic data alone. Seismic imaging in the offshore Nile Delta is often degraded by velocity heterogeneities, tuning effects in thin beds, and multiple reflections associated with Messinian evaporites, all of which limit the effectiveness of conventional amplitude-based interpretation (Al-Sharhan and Salah 1997; Sedki et al. 2025a, b). Consequently, deterministic approaches such as post-stack seismic inversion have been widely applied to convert seismic reflection data into quantitative elastic properties, most notably acoustic impedance (AI), which provides a more direct link to lithology and pore-fluid content (Russell 1988). Although inversion significantly enhances interpretability, its predictive capability may still be constrained by sparse well control, uncertainty in low-frequency models, and non-uniqueness of inversion solutions (Abdel-Fattah et al. 2022).

In recent years, machine learning and artificial intelligence techniques have been increasingly integrated with seismic interpretation to overcome some of these limitations (Leisi and Saberi 2023; Leisi and Shad Manaman 2024; Abdel-Fattah et al. 2025; Amir et al. 2025a, b, c a, b; Reda et al. 2025b). Neural-network-based approaches, including probabilistic neural networks (PNNs), are particularly attractive because they can capture non-linear relationships between multiple seismic attributes and target reservoir properties derived from well logs (Hampson et al. 2001; Smith and Treitel 2010; Zheng et al. 2014; Leisi et al. 2024a, b; Amir et al. 2025a, b, c; Leisi et al. 2026a, b). By training on well-calibrated seismic data, PNNs can predict petrophysical parameters such as clay volume, porosity, and water saturation away from wells, thereby improving spatial coverage and reducing interpreter bias. However, the reliability of such predictions depends critically on robust training, validation, and geological consistency.

This study adopts an integrated workflow that combines post-stack, model-based acoustic impedance inversion with PNN-driven seismic attribute analysis to enhance reservoir characterization in the Denise gas field. Acoustic

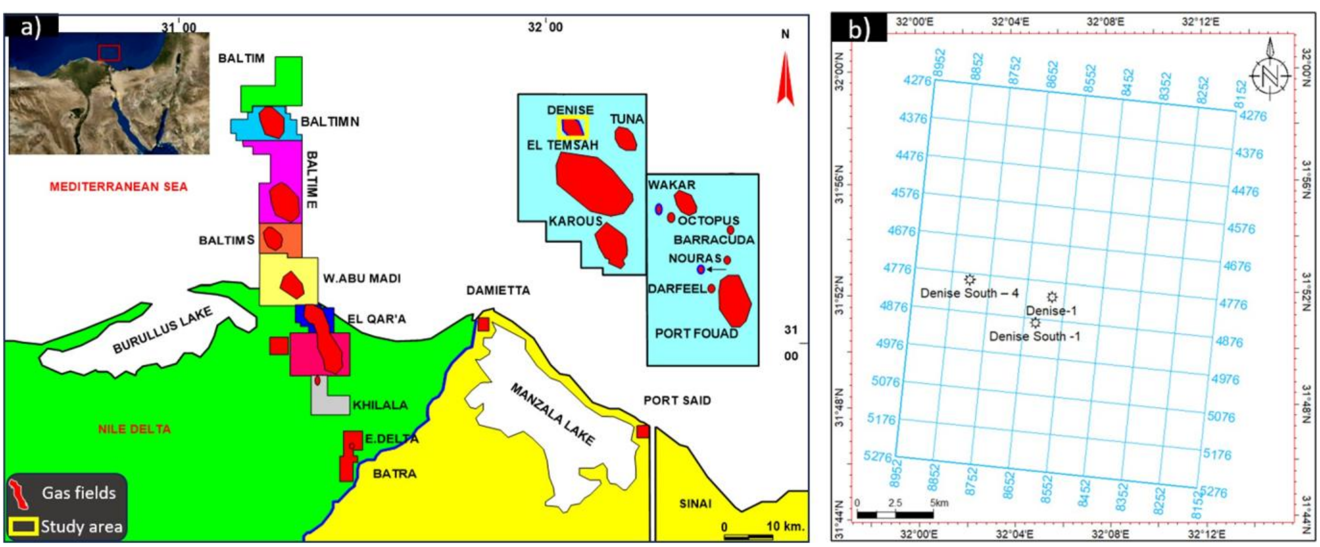

Fig. 1 **a** Regional map of the Nile Delta showing the location of major oil and gas fields, highlighting the position of the Denise Gas Field within the eastern offshore Nile Delta (Egypt). **b** Detailed map of the study area illustrating the 3D seismic survey grid and the locations of the analyzed wells (Denise − 1, Denise South-1, and Denise South-4)

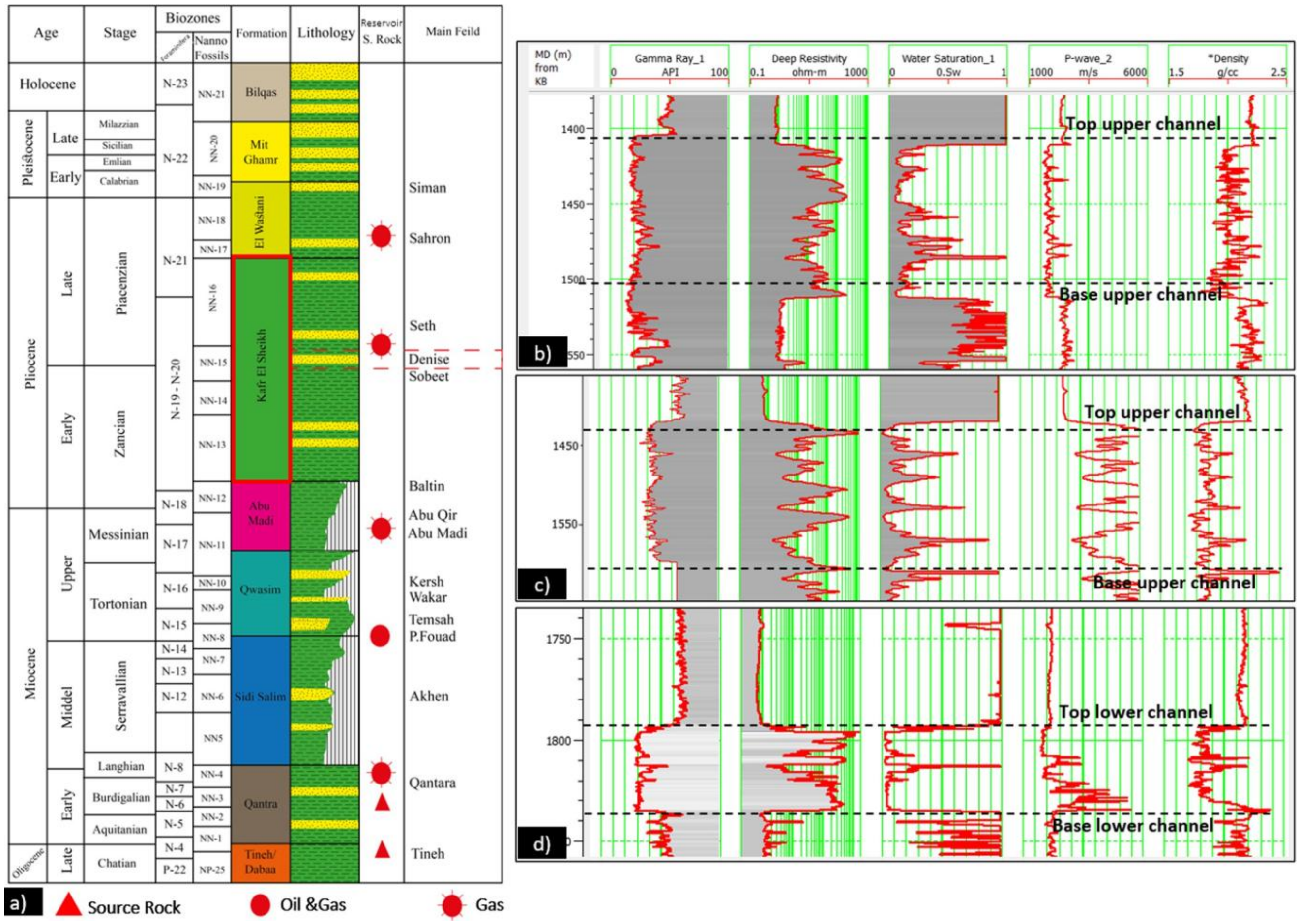

Fig. 2 **a** Stratigraphic column of the Miocene–Pleistocene succession in the eastern Nile Delta showing the Rosetta, Kafr El-Sheikh, El Wastani, and Baltim formations. **b**, **c** Representative well logs from Denise South-1 illustrating the upper and lower channel reservoirs within the Kafr El-Sheikh Formation, based on gamma ray, resistivity, water saturation, P-wave velocity, and density logs

Table 1 Petrophysical summary of the upper and lower channel reservoirs in the Denise Field

Well	Reservoir	Gross (m)	Net pay (m)	Net/Gross (m)	V_{sh} (%)	PHIE (%)	S_w (%)
D-01	Upper channel	278	94	0.34	23	18	38
DS-04		170	130	0.77	18	31	19
DS-01	Lower channel	57	38.5	0.67	17	29	21

impedance inversion is first used to establish a physically constrained framework for lithological discrimination and to highlight impedance contrasts associated with gas-bearing channel sands. Subsequently, a carefully selected suite of seismic attributes is employed to train PNN models to predict key petrophysical properties, including shale volume (V_{sh}), effective porosity (Φ_e), and water saturation (S_w). The integration of deterministic inversion results with data-driven neural network predictions aims to leverage the strengths of both approaches: the geological plausibility and interpretability of inversion, and the improved spatial resolution and predictive power from machine learning.

The primary objectives of this work are to: (1) generate and validate an acoustic impedance volume capable of resolving lithological variations relevant to the Denise reservoirs; (2) develop and validate PNN models for predicting V_{cl}, Φ_e, and S_w from seismic attributes using rigorous training and blind testing; and (3) integrate the resulting volumes to delineate reservoir fairways, identify zones of favorable reservoir quality, and support development and infill drilling decisions. By demonstrating the effectiveness of this integrated inversion–PNN workflow, the study contributes to advancing reservoir characterization practices in complex clastic systems of the offshore Nile Delta and comparable gas provinces worldwide.

2 The geologic setting of the Nile Delta: a rising global gas province

The Nile Delta Basin has rapidly emerged as one of the most prolific gas provinces in the Mediterranean region, supported by large discovered reserves and substantial

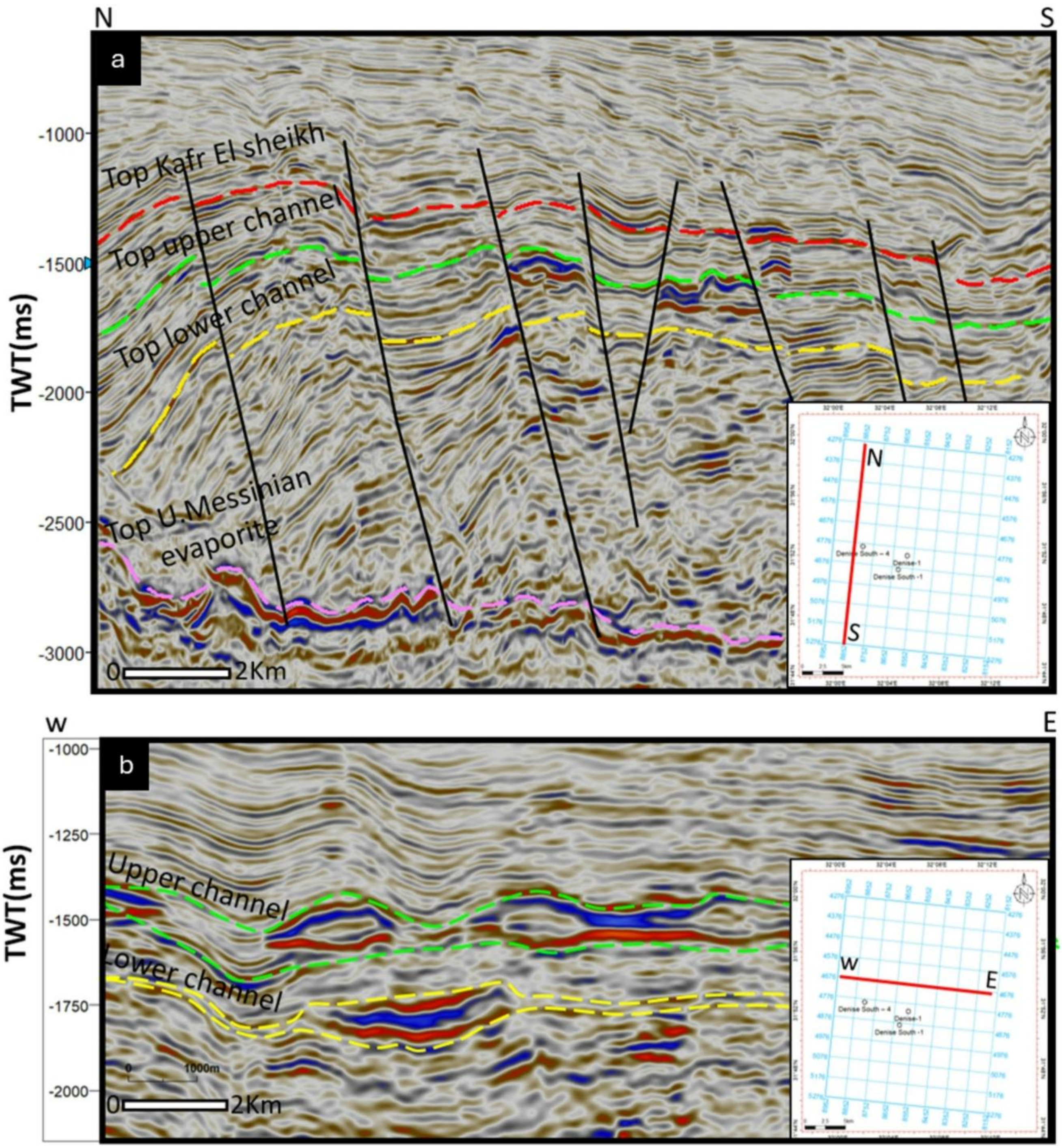

Fig. 3 Interpreted seismic sections in the Denise Field. **a** N–S seismic section through the Pliocene succession showing listric normal faults and key horizons, including the top Kafr El-Sheikh Formation, upper and lower channels, and the top Messinian evaporites. **b** E–W seismic section illustrating the geometry and continuity of the upper and lower channel systems within the study area

remaining exploration potential (Sarhan 2022; Radwan et al. 2024). Recent assessments emphasize significant "Yet-to-Find" volumes, reinforcing the strategic importance of the basin as a long-term gas province. The depositional evolution of the Nile Delta Basin has been strongly influenced by repeated tectonic episodes and Mediterranean Sea-level fluctuations, which collectively controlled sediment supply, accommodation space, and basin architecture (Ayyad and Darwish 1996). As a result, the basin hosts a complex stratigraphic framework shaped by the interaction of fluvial, marine, and deep-marine depositional systems over geological time (Rizzini et al. 1978; Sestini 1989; Reda et al. 2024d).

2.1 Stratigraphic evolution: from Messinian evaporites to pliocene shales

The sedimentary succession of the Nile Delta spans the Miocene to Pleistocene, with the Pliocene interval representing the most critical phase for hydrocarbon accumulation (Fig. 2a). Stratigraphically, the basin records a progressive transition from fluvial–deltaic environments to deep-marine settings, driven by eustatic sea-level variations and changes in sediment flux (Harwood et al. 1998; Samuel et al. 2002; Court 2009; Kirschbaum et al. 2010; Metwally et al. 2023; Anwar et al. 2025). These depositional shifts generated stacked reservoir–seal pairs that underpin the basin's prolific gas productivity.

During the Late Miocene (Messinian), fluvio-marine deposition dominated the Central Sub-basin, leading to the accumulation of the Abu Madi and Qawasim formations (Sarhan 2022; Shehata et al. 2023; Elgendy et al. 2024). These units are characterized by sand-prone channel fills that form some of the basin's most important gas reservoirs. In contrast, the Eastern Sub-basin experienced the deposition of the Rosetta Formation, comprising thick evaporitic sequences associated with the Mediterranean isolation during the Messinian Salinity Crisis (Mascle 2019). These evaporites now function as regionally effective seals, significantly enhancing trap integrity and hydrocarbon preservation in underlying reservoirs.

The Early Pliocene marks a major marine transgression following the reflooding of the Mediterranean Sea, resulting in the widespread deposition of the Kafr El-Sheikh Formation (Shehata et al. 2023). This unit consists predominantly of thick, deep-marine shales that serve as both prolific source rocks and effective regional seals. The formation exhibits notable thickness variations across the basin, with enhanced accumulation along the eastern flank, attributed to longshore paleocurrents that transported

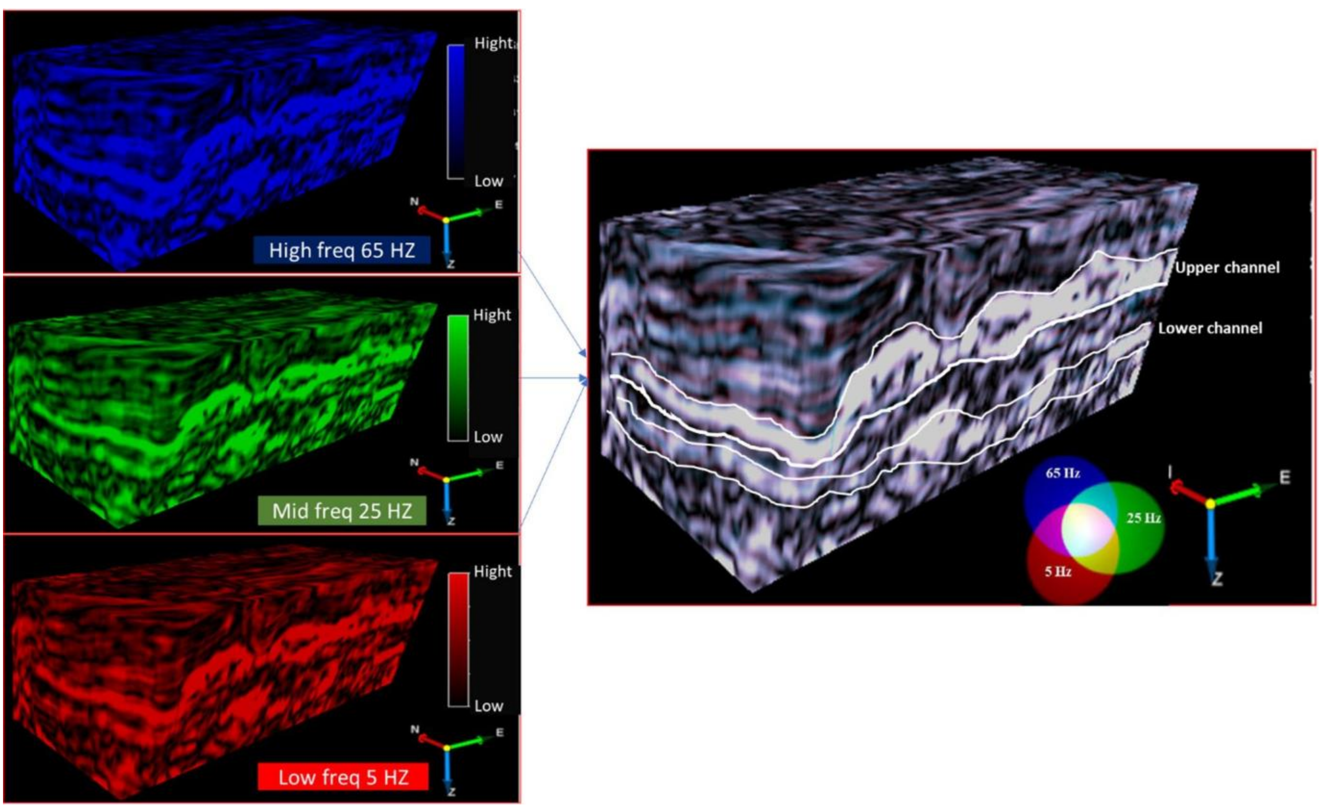

Fig. 4 Color-blended spectral decomposition volume over the upper channel in the Denise Field, combining low (5 Hz), mid (25 Hz), and high (65 Hz) frequency components. The blended response enhances channel geometry and continuity, clearly delineating the upper and lower channel fairways and highlighting improved channel definition toward the western sector (modified after Negm 2018)

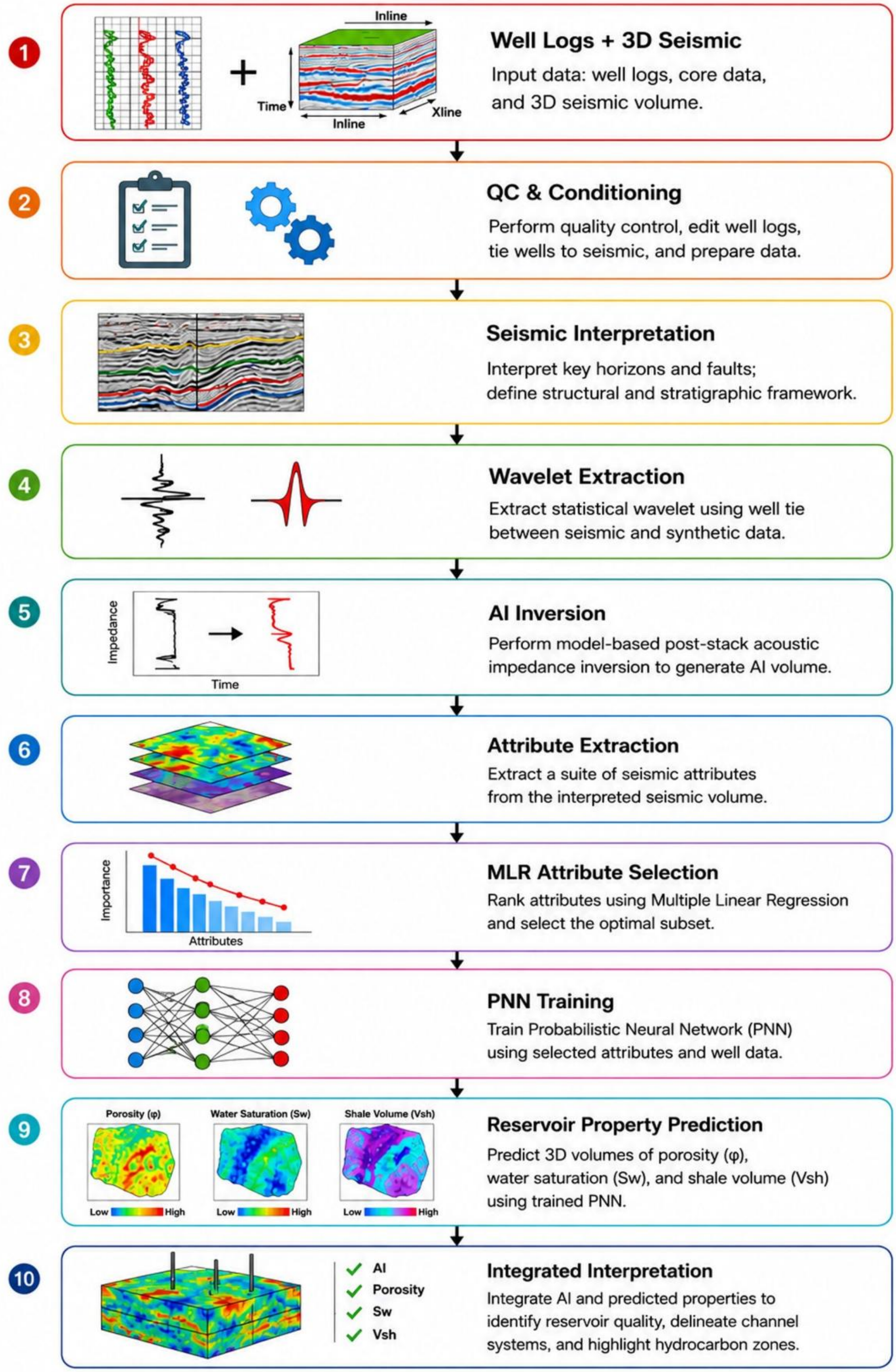
1
Inline
Time
Inline
Xline
Well Logs + 3D Seismic
Input data: well logs, core data, and 3D seismic volume.
2
QC & Conditioning
Perform quality control, edit well logs, tie wells to seismic, and prepare data.
3
Seismic Interpretation
Interpret key horizons and faults; define structural and stratigraphic framework.
4
Wavelet Extraction
Extract statistical wavelet using well tie between seismic and synthetic data.
5
Impedance
Time
AI Inversion
Perform model-based post-stack acoustic impedance inversion to generate AI volume.
6
Attribute Extraction
Extract a suite of seismic attributes from the interpreted seismic volume.
7
Importance
Attributes
MLR Attribute Selection
Rank attributes using Multiple Linear Regression and select the optimal subset.
8
PNN Training
Train Probabilistic Neural Network (PNN) using selected attributes and well data.
9
Porosity (φ)
Water Saturation (Sw)
Shale Volume (Vsh)
Low High
Low High
Low High
Reservoir Property Prediction
Predict 3D volumes of porosity (φ), water saturation (Sw), and shale volume (Vsh) using trained PNN.
10
AI
Porosity
Sw
Vsh
Integrated Interpretation
Integrate AI and predicted properties to identify reservoir quality, delineate channel systems, and highlight hydrocarbon zones.

Fig. 5 Integrated workflow combining seismic interpretation, post-stack inversion, and machine learning (Neural Networks) for reservoir characterization in the Denise Gas Field (Offshore Nile Delta), Egypt

fine-grained sediments eastward. In the eastern Nile Delta, including the Denise Field, the Kafr El-Sheikh Formation directly overlies Miocene fluvio-marine deposits and plays a key role in the architecture of the petroleum system (Abd El Aal et al. 1994; Kirschbaum et al. 2010).

By the Late Pliocene, renewed delta progradation led to the deposition of the El Wastani Formation, composed mainly of deltaic to shallow-marine sands with excellent reservoir properties (Selim et al. 2024). Overlying Pleistocene deposits, although less explored, contain additional clastic reservoirs that represent promising targets for future exploration. Of particular significance are the stacked deep-marine turbidite channels developed during the Pliocene–Pleistocene. These channels comprise multiple sand-rich lobes deposited by sediment gravity flows within confined submarine canyon systems. Well data indicate exceptional reservoir quality (Table 1), with gross thicknesses reaching ~ 165 m, net pay up to ~ 50 m, average porosity around 28%, and relatively low water saturation (Fig. 2). Such characteristics highlight the importance of turbidite systems as major contributors to the Nile Delta's gas resources.

2.2 Structural framework and exploration implications

The structural framework of the Nile Delta Basin has been extensively investigated by numerous authors (Orwig 1980, 1982; Doherty et al. 1988; Sestini 1989; Abdel Aal et al. 1994; Dolson et al. 2019; Negm et al. 2025). The basin represents a classic passive-margin setting that developed through the interaction between the African Plate and the Tethyan oceanic domain. Its present-day structural configuration reflects a prolonged history of regional subsidence, rapid sediment progradation, and post-Miocene tectonic adjustments that collectively shaped basin architecture and petroleum system development.

Structurally, the Nile Delta Basin is broadly subdivided into two major depocenters with contrasting geological characteristics (Dolson et al. 2019). The Central Sub-basin is dominated by fluvio-marine clastic deposits, whereas the Eastern Sub-basin is characterized by thick evaporitic successions related to the Messinian Salinity Crisis. This basin-scale segmentation exerts a fundamental control on stratigraphic thickness, facies distribution, and trap styles across the delta. Extensional tectonics associated with the Late Miocene Messinian event, followed by continued Pliocene subsidence, resulted in the development of numerous listric normal faults, growth faults, and associated rollover anticlines. These structures created pronounced structural highs and lows, leading to strong reservoir compartmentalization and the formation of distinct petroleum systems. Within the Pliocene succession, seismic interpretation reveals the widespread occurrence of listric normal faults with large rollover anticlines, particularly evident in north–south-oriented seismic sections (Fig. 3a). These fault systems accommodated differential sediment loading and shale mobility, enhancing accommodation space and influencing sediment routing into deeper parts of the basin. The interaction between fault-controlled subsidence and high sediment supply played a critical role in focusing sediment gravity flows and controlling the geometry of deep-marine depositional systems.

Among the most significant structural–stratigraphic features in the eastern offshore Nile Delta are the deep-marine turbidite channels, commonly referred to as the upper and lower channels. These channel systems constitute major exploration and development targets and display a combined stratigraphic–structural trapping style (Fig. 3b). Deposited under restricted deep-marine conditions, the channels are influenced by subtle structural tilting and faulting, which enhance trap formation and reservoir compartmentalization. Consequently, they represent key contributors to the delta's gas production, particularly in fields such as Denise (Abd El Aal et al. 1994).

Advanced seismic attribute analysis has further refined the understanding of these channel systems. Spectral decomposition of the upper and lower channels shows that channel fairways are more clearly defined toward the western termination. At the same time, lateral separation and segmentation become more pronounced toward the eastern sector (Fig. 4), reflecting variations in sediment supply, confinement, and structural control (Negm 2018). These observations highlight the strong coupling between depositional processes and structural evolution in governing reservoir distribution and connectivity.

3 Materials and methods

This study follows an integrated workflow for reservoir characterization that combines well-log analysis, seismic interpretation, acoustic impedance inversion, and machine-learning-based property prediction (Fig. 5). The workflow begins with data acquisition and quality control of available well logs and 3D seismic data, followed by petrophysical evaluation to estimate shale volume (V_{Sh}), effective porosity (Φ_e), water saturation (S_w), and acoustic impedance (AI). Subsequently, seismic interpretation and horizon mapping were performed to delineate the upper and

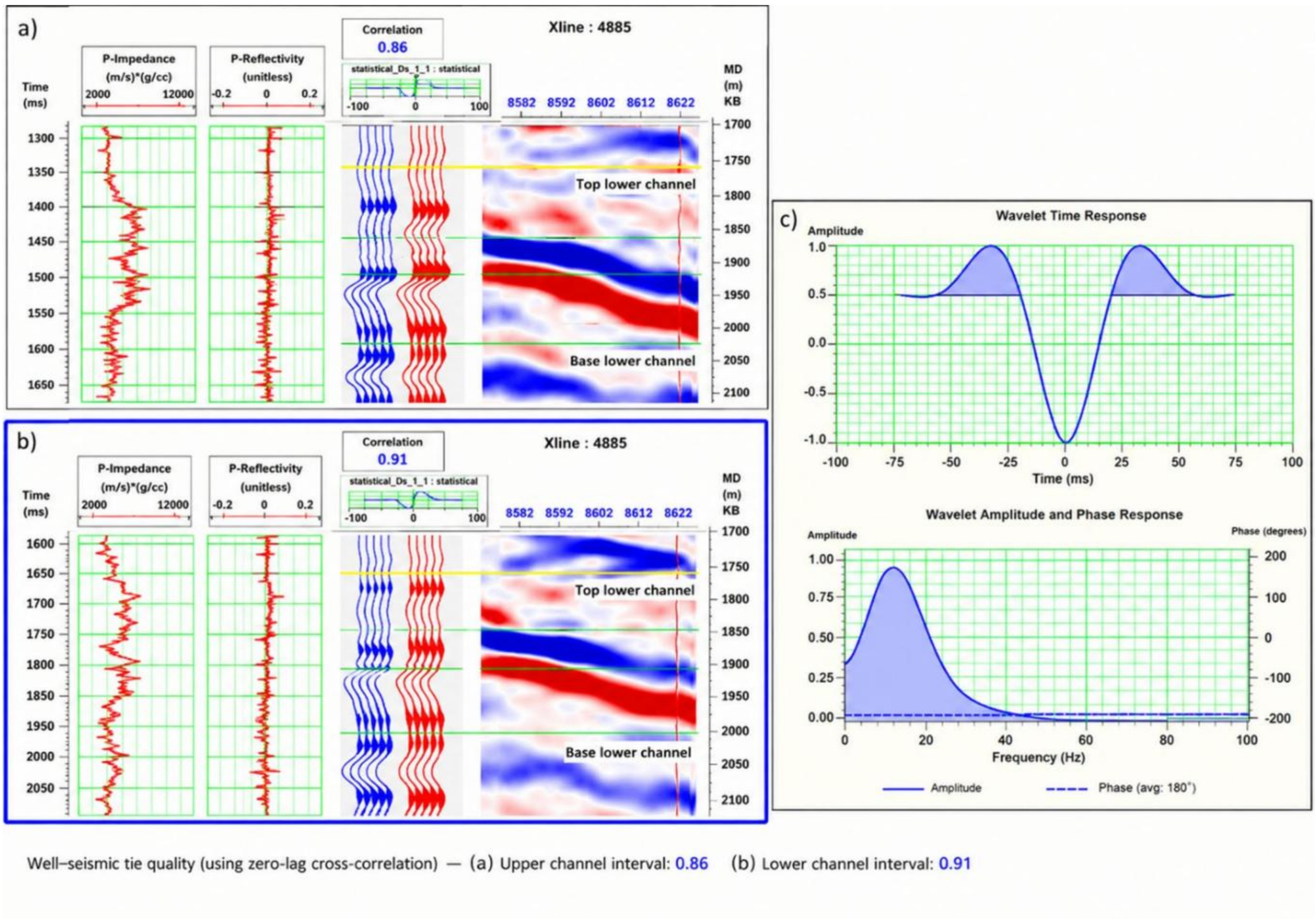

Fig. 6 **a**, **b** Well-to-seismic ties at the Denise wells, showing P-impedance and reflectivity logs with reservoir intervals highlighted. Blue traces represent synthetic seismograms generated using the extracted statistical wavelet, while red traces show the corresponding composite seismic amplitudes, illustrating a good match across the upper and lower channel intervals. **c** Extracted statistical wavelet, including the time response and the amplitude and phase spectra (phase ≈ 180°), used for post-stack seismic inversion

lower channel reservoirs. Model-based post-stack acoustic impedance inversion was then conducted and validated using well-to-seismic ties and impedance comparisons at well locations. Finally, probabilistic neural network (PNN) models were developed using optimized seismic attributes to predict reservoir properties across the field. The complete workflow is summarized in Fig. 5 and provides a systematic framework for integrating well and seismic data to improve reservoir characterization and reduce interpretation uncertainty.

3.1 Data and pre-processing

This study integrates wireline log and post-stack seismic datasets to support quantitative reservoir characterization in the Denise Field. Wireline log data were available from three vertical wells— Denise − 1, Denise South-1, and Denise South-4—including gamma-ray (GR), resistivity, density, and sonic logs. All log suites underwent rigorous quality control procedures to ensure data integrity prior to analysis. Environmental corrections were applied to account for borehole-related effects such as washouts, tool recentering, and possible instrument drift, thereby improving the reliability of the derived petrophysical properties.

The seismic dataset comprises a post-stack 3D seismic volume acquired in 2003 and processed by PGS in 2004. This dataset provides the primary framework for seismic inversion and seismic-to-well integration. The available seismic volumes were suitable for constructing the initial low-frequency model through kriging and were also employed as external attributes in subsequent neural-network analyses. The original seismic data, sampled at 4 ms, were resampled and band-pass filtered to 120–130 Hz to enhance vertical resolution and improve consistency with the well log data.

Statistical wavelet extraction was carried out using a 300 ms time window spanning from 1200 ms to 1750 ms, with a 50 ms taper applied at the window edges and a

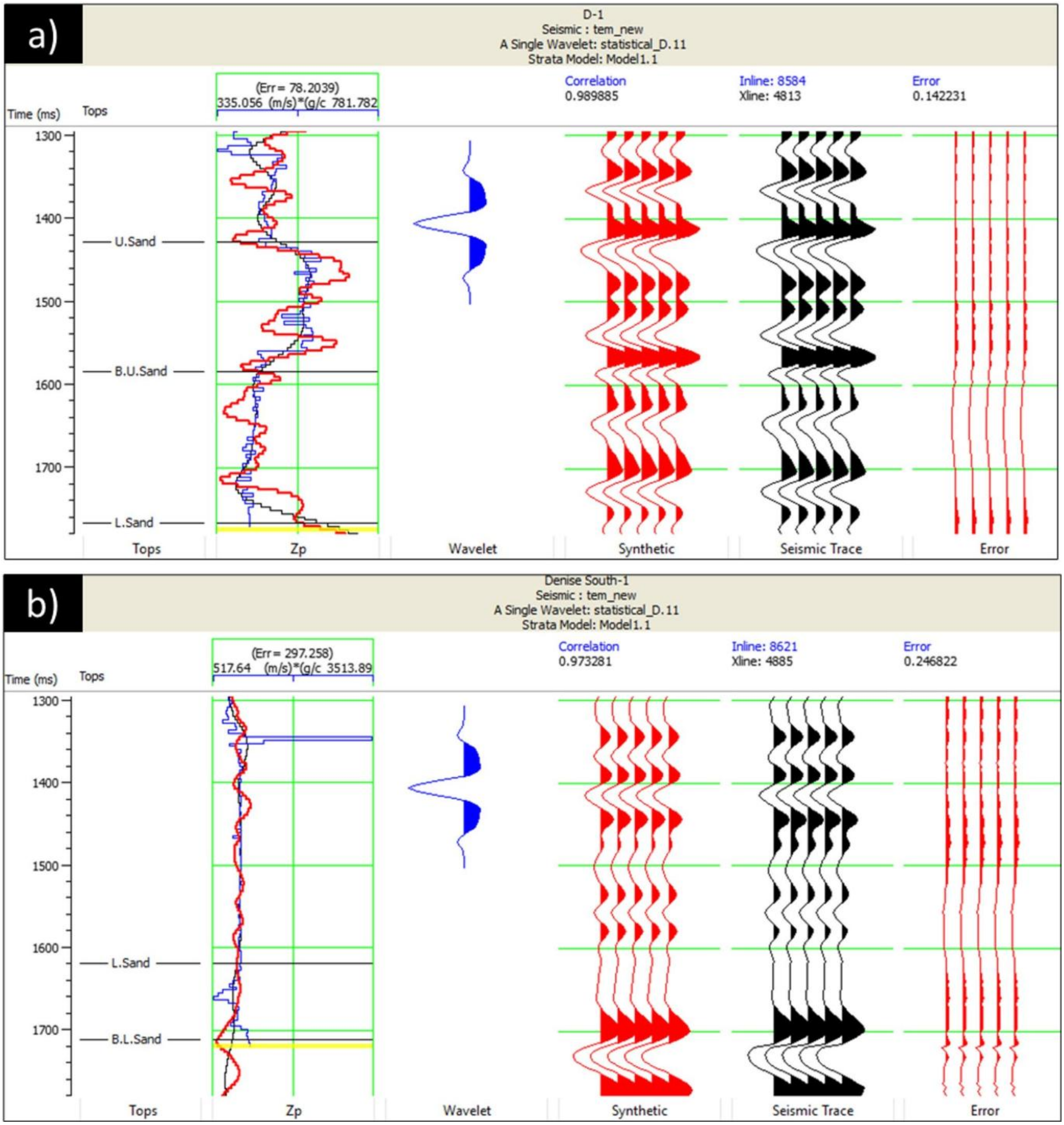

Fig. 7 Post-stack acoustic impedance inversion results at the Denise-1 **a** and Denise South-1 **b** wells. The inverted P-impedance logs (red) closely match the original well-log impedance (blue). Synthetic seismic traces generated from the inversion (red) show an excellent correlation with the stacked seismic traces (black), reaching ~ 0.99 at DENISE-1 and ~ 0.97 at Denise South-1. The error track on the right represents the residual misfit between the synthetic and observed seismic data

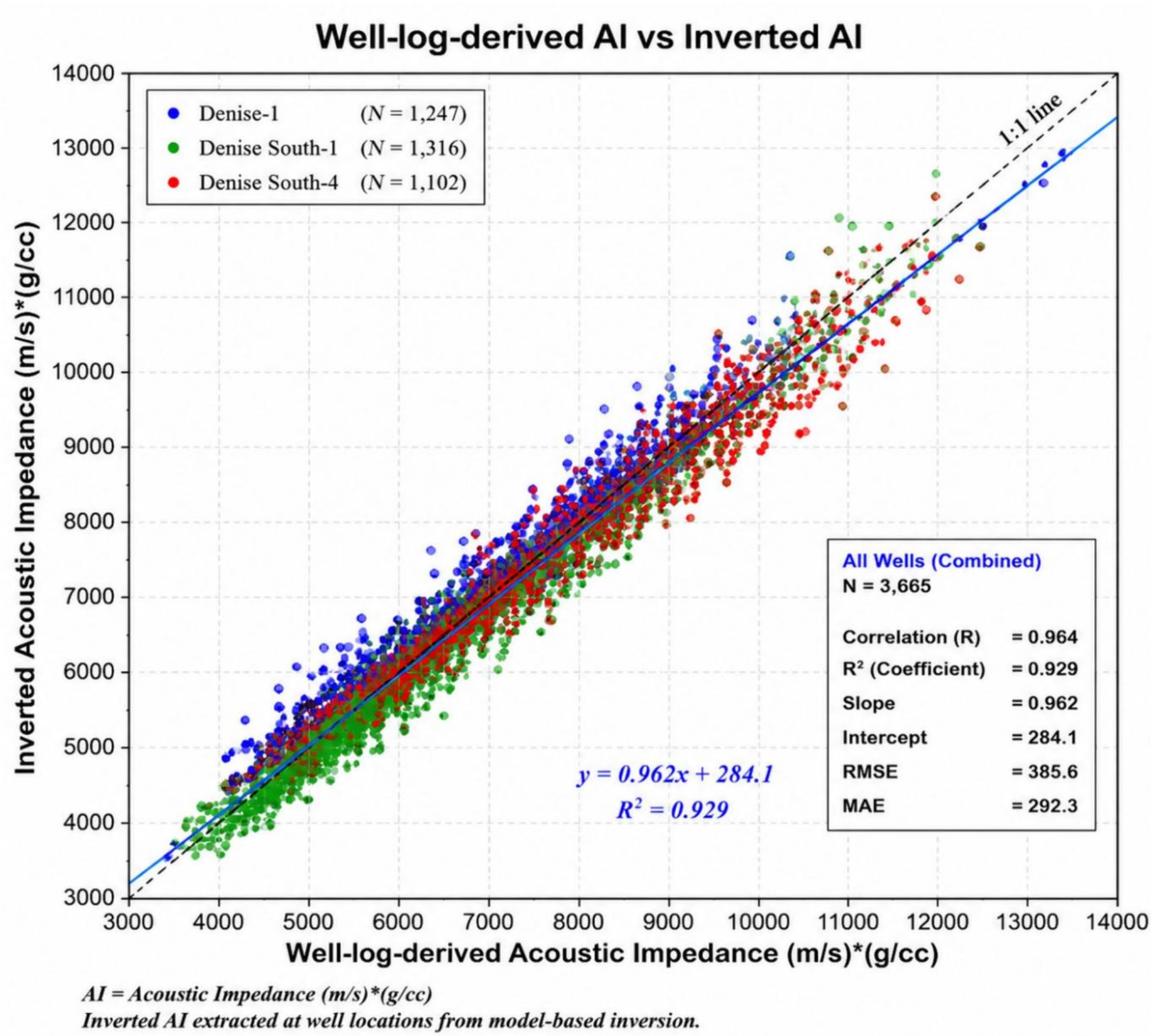

Fig. 8 Cross-plot of well-log-derived acoustic impedance (AI) versus inverted acoustic impedance extracted from the model-based inversion at the Denise-1, Denise South-1, and Denise South-4 wells. The strong clustering of data points around the 1:1 line and the high correlation coefficient ($R = 0.964$; $R^2 = 0.929$) demonstrate excellent agreement between measured and inverted AI values, confirming the reliability and accuracy of the inversion results for reservoir characterization

phase rotation of 180° (Fig. 6c). The extracted wavelet was validated through the generation of synthetic seismograms, which were compared against the real seismic traces at the Denise − 1 and Denise South-1 well locations (Fig. 6a, b). The synthetic-to-seismic ties were iteratively optimized by refining the time–depth relationships and adjusting wavelet parameters, resulting in a robust match between synthetic and observed seismic data (Smith and Treitel 2010; Leisi and Shad Manaman 2025a). This careful pre-processing and calibration ensured a reliable linkage between the well and seismic domains, providing a solid foundation for subsequent seismic inversion and neural-network-based reservoir property prediction (Zheng et al. 2014; Leisi and Shad Manaman 2025b).

3.2 Post-stack acoustic impedance inversion

A model-based post-stack seismic inversion approach was applied to generate acoustic impedance (AI) volumes, using well-derived impedance trends as primary constraints (Fig. 7). The inversion workflow began with conditioning the well log data to ensure compatibility with the seismic bandwidth and sampling interval (Latimer et al. 2000). Sonic and density logs were resampled to the seismic scale

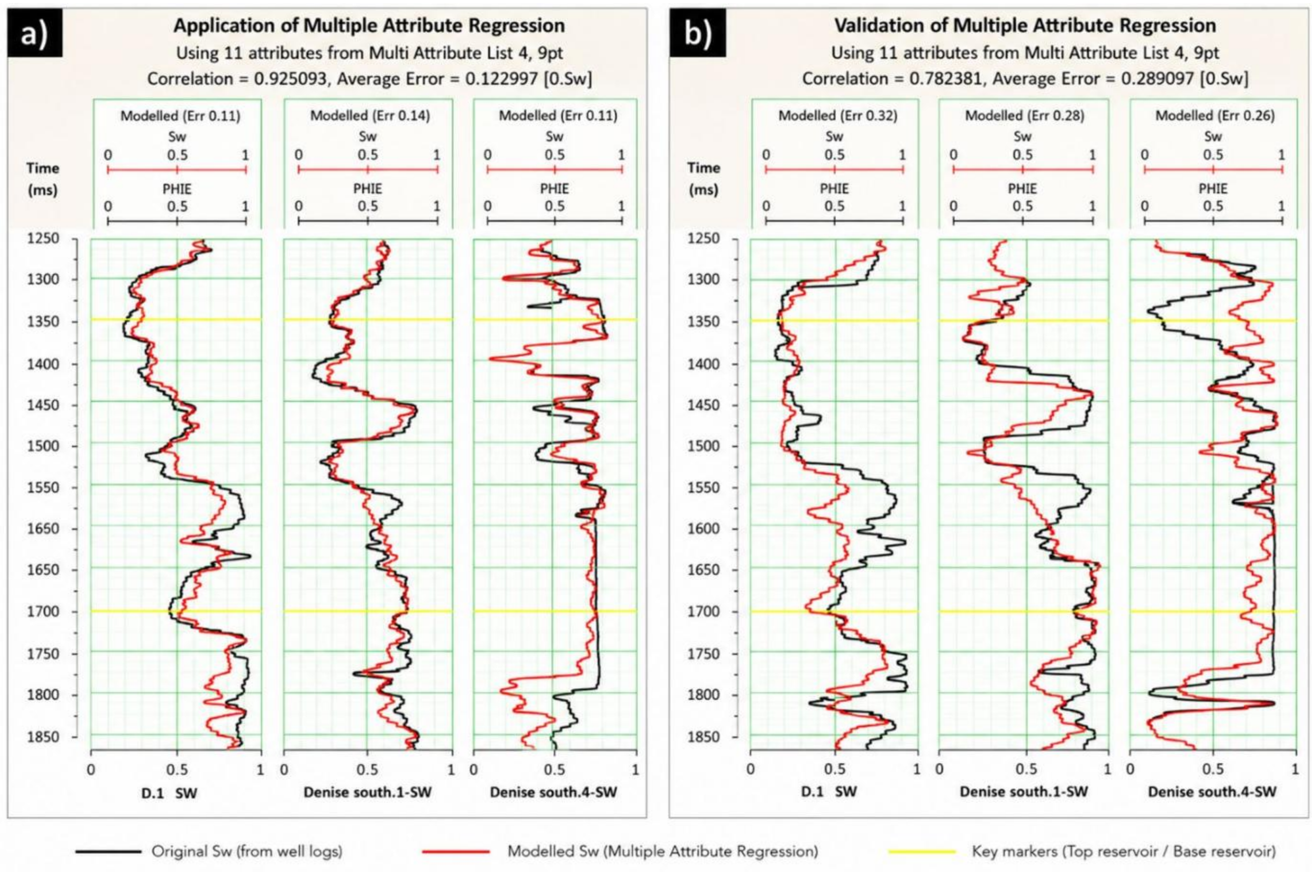

Fig. 9 Comparison between measured and predicted water saturation (S_w) logs using **a** multi-attribute linear regression and **b** probabilistic neural network (PNN). Black curves represent measured S_w logs, while red curves show predicted values for the DENISE-1, Denise South-1, and Denise South-4 wells. The results demonstrate improved prediction accuracy and higher correlation using the PNN approach compared to multi-attribute regression

and low-pass filtered to restrict their frequency content to that of the post-stack seismic amplitude data (120–130 Hz). This step minimized aliasing effects during down-sampling and ensured spectral consistency between the well and seismic domains. A mild smoothing operator was subsequently applied to the filtered logs to suppress residual spikes while preserving meaningful impedance variations.

Wavelet estimation was carried out using a statistical extraction technique based solely on post-stack seismic amplitude data. This approach relies on the autocorrelation of seismic traces to derive the wavelet, without explicitly calculating the phase spectrum; therefore, the wavelet phase was provided as a user-defined parameter. Several wavelet-extraction scenarios were tested to assess sensitivity and optimize inversion performance. Three taper lengths—40, 50, and 60 ms—were evaluated using a constant total wavelet length of 150 ms. Among these options, the 50 ms taper produced the most stable and highest correlation results and was therefore selected for the final inversion. All extracted wavelets were generated using the full-waveform method, and the resulting wavelets exhibited phases close to 180°, consistent with the polarity of the seismic data.

The inversion process involved matching synthetic seismic traces generated from the inverted impedance models to the actual seismic data at well locations (Smith and Treitel 2010; Zheng et al. 2014). This matching was achieved through pattern-matching techniques, supported by pre-defined well-log markers to ensure accurate time alignment and stratigraphic consistency. The inversion results for the time interval from 1300 to 1700 ms are shown in Fig. 6a and b for the Denise-1 and Denise South-1 wells, respectively. For each well, the first track displays the inverted acoustic impedance curve (solid red) overlaid on the original impedance log derived from well data (solid blue), with the initial low-frequency impedance model shown as a solid black line. The second track presents the synthetic seismic trace generated from the inversion result (red), while the third track shows the original composite seismic trace at the well location (black). The fourth track represents the error trace, highlighting the residual misfit between the synthetic and observed seismic data.

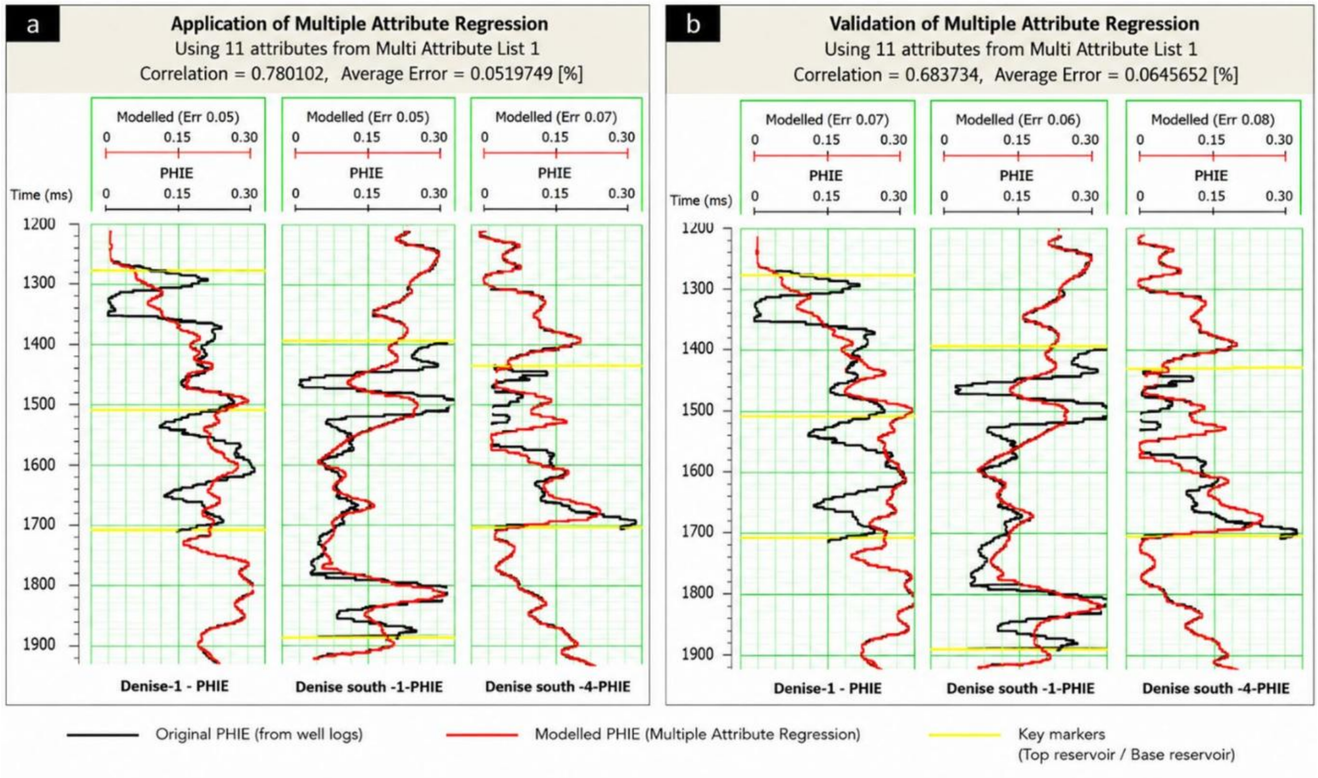

Fig. 10 **a** The application of the multi-attribute linear regression transforms. Measured effective porosity logs (in black) and the predicted ones (in red). The normalized correlation coefficient for all the wells is 0.78%. **b** Validation of the multi-attribute linear regression at the training wells: the normalized correlation coefficient across all wells is 0.68%

The cross-plot demonstrates an excellent agreement between the well-log-derived acoustic impedance and the inverted acoustic impedance extracted from the model-based inversion (Fig. 8). Data points from the three wells cluster closely around the 1:1 line, indicating that the inversion successfully reproduces the impedance variations observed in the well logs. The high correlation coefficient ($R = 0.964$) and coefficient of determination ($R^2 = 0.929$) confirm the robustness and reliability of the inversion results, providing strong confidence in the use of the inverted acoustic impedance volume for reservoir characterization and subsequent prediction of petrophysical properties.

3.3 Probabilistic neural network (PNN) for property prediction

A probabilistic neural network (PNN) was applied to predict key petrophysical properties (Figs. 9, 10 and 11), including effective porosity and water saturation, from seismic attribute volumes following the methodology of Hampson et al. (2001) and Singh et al. (2016). The PNN approach is well-suited for seismic-based property prediction because it provides a statistically rigorous framework for non-linear regression while minimizing overfitting by explicitly optimizing validation error. The adopted workflow consists of four sequential steps.

In the first step, well-log conditioning was performed to ensure consistency between well data and seismic attributes. Log-derived petrophysical properties were resampled to the seismic time scale and aligned with the corresponding seismic traces at well locations, preserving the statistical relationships between seismic responses and reservoir properties. This conditioning step is essential for reducing scale mismatch and ensuring reliable neural network training.

In the second step, the most effective set of seismic attributes for predicting each target reservoir property was identified using multi-linear regression (MLR). The regression analysis was applied between the training values at the wells and a suite of candidate seismic attributes, and those attributes yielding the lowest prediction error were retained. This stepwise regression procedure allows ranking

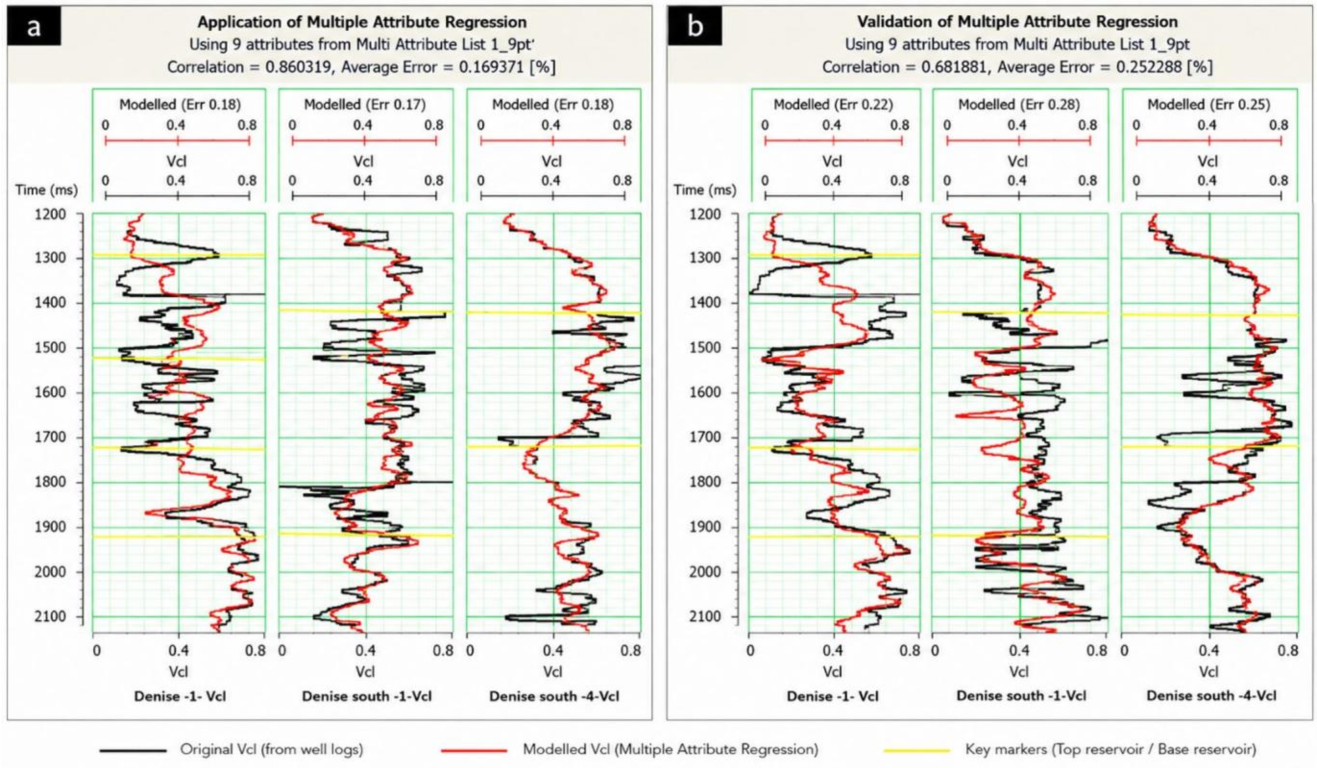

Fig. 11 **a** The application of the multi-attribute linear regression transforms. Measured clay volume logs (in black) and the predicted ones (in red). The normalized correlation coefficient for all the wells is 0.86%. **b** Validation of the multi-attribute linear regression at the training wells: the normalized correlation coefficient across wells is 0.68%

Table 2 Stepwise multilinear regression results for predicting clay volume (V_{cl}) using seismic attributes, showing training and validation errors; the minimum validation error is achieved using eight attributes

No	Petro-physical parameter	Seismic attribute	Training error	Validation error
1	Vcl	Integrated absolute amplitude	0.272	0.315
2	Vcl	Apparent polarity	0.255	0.304
3	Vcl	Average frequency	0.228	0.366
4	Vcl	Amplitude weighted cosine phase	0.215	0.426
5	Vcl	Average frequency	0.201	0.384
6	Vcl	Integrated	0.191	0.348
7	Vcl	Amplitude weighted phase	0.182	0.381
8	Vcl	Instantaneous frequency	0.176	0.255
9	Vcl	Filter 5/10–15/20	0.169	0.252
10	Vcl	Integrated absolute amplitude	0.164	0.256

Table 3 Stepwise multilinear regression results for predicting porosity using seismic attributes, showing training and validation errors; the minimum validation error is achieved using the tenth attribute

No	Petrophysical parameter	Seismic attribute	Training error	Validation error
1	Porosity	X-coordinate	0.0739	0.0749
2	Porosity	Quadrature trace	0.069	0.0752
3	Porosity	Integrate (variance)	0.066	0.0735
4	Porosity	Average frequency	0.063	0.0701
5	Porosity	Integrated absolute amplitude	0.061	0.0744
6	Porosity	Amplitude envelope	0.058	0.0654
7	Porosity	Filter 15/20–25/30	0.057	0.0650
8	Porosity	integrate	0.056	0.0658
9	Porosity	Filter 5/10–15/20	0.0555	0.0670
10	Porosity	Filter 5/10–15/20 (am_cn)	0.053	0.0649
11	Porosity	(R_Ac.Im)**2	0.051	0.0645

attributes by their predictive contribution while reducing multicollinearity and eliminating redundant inputs.

In the third step, the convolutional multi-linear regression coefficients were applied to seismic traces from locations away from the training wells to generate preliminary volumes of predicted reservoir parameters. These regression-based volumes provide an initial spatial estimate of property distribution and serve as an important benchmark for evaluating the added value of the neural-network approach.

In the fourth step, the number and order of attributes selected via multiple linear regression were used as inputs

Table 4 Stepwise multilinear regression results for predicting water saturation using seismic attributes, showing training and validation errors; the minimum validation error is achieved using the twelfth attribute

No	Petrophysical parameter	Seismic attribute	Training error	Vali-dation error
1	Water saturation	Apparent polarity	0.282	0.296
2	Water saturation	1/(variance)	0.266	0.309
3	Water saturation	Quadrature trace	0.251	0.305
4	Water saturation	Derivative instantaneous amplitude	0.236	0.300
5	Water saturation	Average frequency	0.222	0.279
6	Water saturation	Dominant frequency	0.212	0.275
7	Water saturation	Apparent polarity	0.199	0.255
8	Water saturation	Average frequency	0.190	0.280
9	Water saturation	Instantaneous phase	0.184	0.262
10	Water saturation	Filter 5/10–15/20	0.177	0.260
11	Water saturation	Quadrature trace	0.169	0.259
12	Water saturation	Instantaneous phase	0.163	0.254
13	Water saturation	Cosine instantaneous phase	0.157	0.268
14	Water saturation	instantaneous	0.151	0.299

Table 5 Quantitative comparison of multi-attribute linear regression performance for predicting clay volume (V_{cl}), effective porosity (PHIE), and water saturation (S_w) using training and validation datasets

Multi-attribute linear regression		Vcl %	PHIE %	Sw %
Training	Correlation	0.78	0.92	0.86
	Error	0.051	0.12	0.16
validation	Correlation	0.68	0.78	0.68
	Error	0.064	0.28	0.25

to the probabilistic neural network for further training. Cross-validation was then performed by predicting well data excluded from the training set, followed by blind-well testing to evaluate model generalization and prediction reliability (Hampson et al. 2001; Todorov 2000).

For the PNN implementation, the available well-log and seismic-attribute samples extracted from the three calibrated wells were randomly divided into training (70%), validation (15%), and blind-testing (15%) datasets to ensure robust model evaluation and reproducibility. The total dataset consisted of several thousand time-sampled data points derived from the reservoir intervals of the upper and lower channels after seismic-to-well alignment and log conditioning. The spread parameter (σ) of the PNN was optimized iteratively through validation-error minimization, and the final adopted value provided the best balance between pre-diction accuracy and model stability. To reduce the risk of overfitting, the workflow incorporated stepwise selection of seismic attributes, independent validation datasets, blind-well testing, and continuous monitoring of prediction errors during training. Model generalization was further evaluated by comparing predicted petrophysical properties against unseen well-log data from excluded intervals and wells, yielding consistently high correlation coefficients and low prediction errors. These procedures confirm that the developed PNN models retained strong predictive capability while maintaining geological consistency away from direct well control.

Although PNNs can be computationally slower than some other neural network architectures, they offer several advantages: independence from initial weight selection, guaranteed convergence, and fully data-driven determination of network parameters (Smith and Treitel 2010; Zheng et al. 2014). In this study, stepwise multi-linear regression was applied to determine the most suitable combinations of seismic attributes for estimating clay volume, effective porosity, and water saturation (Fig. 9). Based on the panels provided in (Fig. 9a, b) a detailed technical interpretation and performance analysis of the Multiple Attribute Regression workflow applied to predict Water Saturation (SW) across three wells: Denise-1, Denise south-1, and Denise south-4. This figure presents a classic side-by-side comparison between the model's performance during training (Application) and its performance on unseen data (Vali-dation). The regression model was constructed using 11 seismic attributes, with a Correlation of 0.92% (an exceptionally high, tight statistical fit) and an Average Error of 0.12%. The true measured well logs are plotted in black, while the mathematically modeled/predicted values are plotted in red. In this training pane, the red curve closely tracks the sharp boundaries and fluid trends of the black log. For example, the low-water-saturation hydrocarbon zones between 1350 ms and 1500 ms are exceptionally well mapped across all three, yielding low localized training errors (0.11 to 0.14).

Furthermore, testing the identical 11-attribute model against independent validation data yielded a correlation coefficient of 0.78 and an average error of 0.28. Tables 2, 3 and 4 summarize the stepwise regression results for the upper and lower channels, showing that the minimum validation error occurs when twelve attributes are included. The final PNN models were trained using optimized seismic attribute volumes—including AI-derived features, integrated amplitude, amplitude envelope, second-derivative instantaneous amplitude, and quadrature trace. Validation results demonstrate reduced prediction errors (e.g., porosity RMSE = 0.066; Table 5), confirming the robustness of the approach. The same workflow was consistently applied to generate effective porosity and clay volume prediction

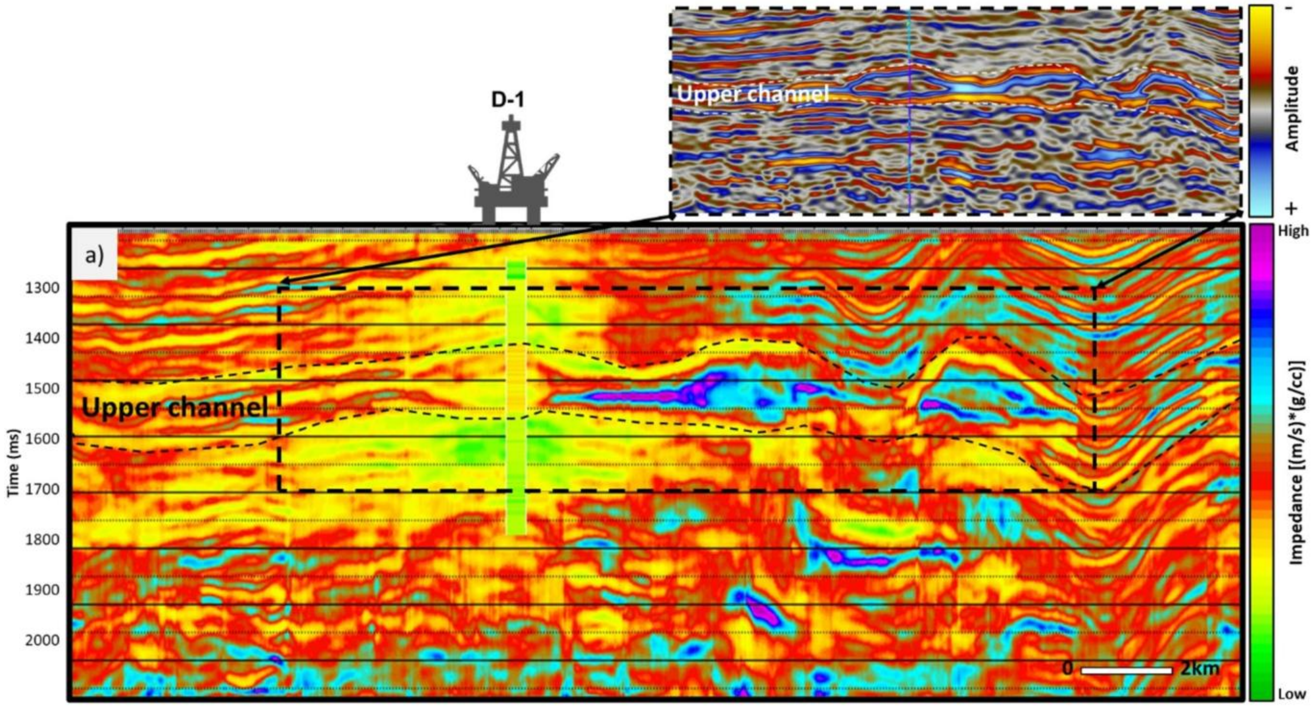

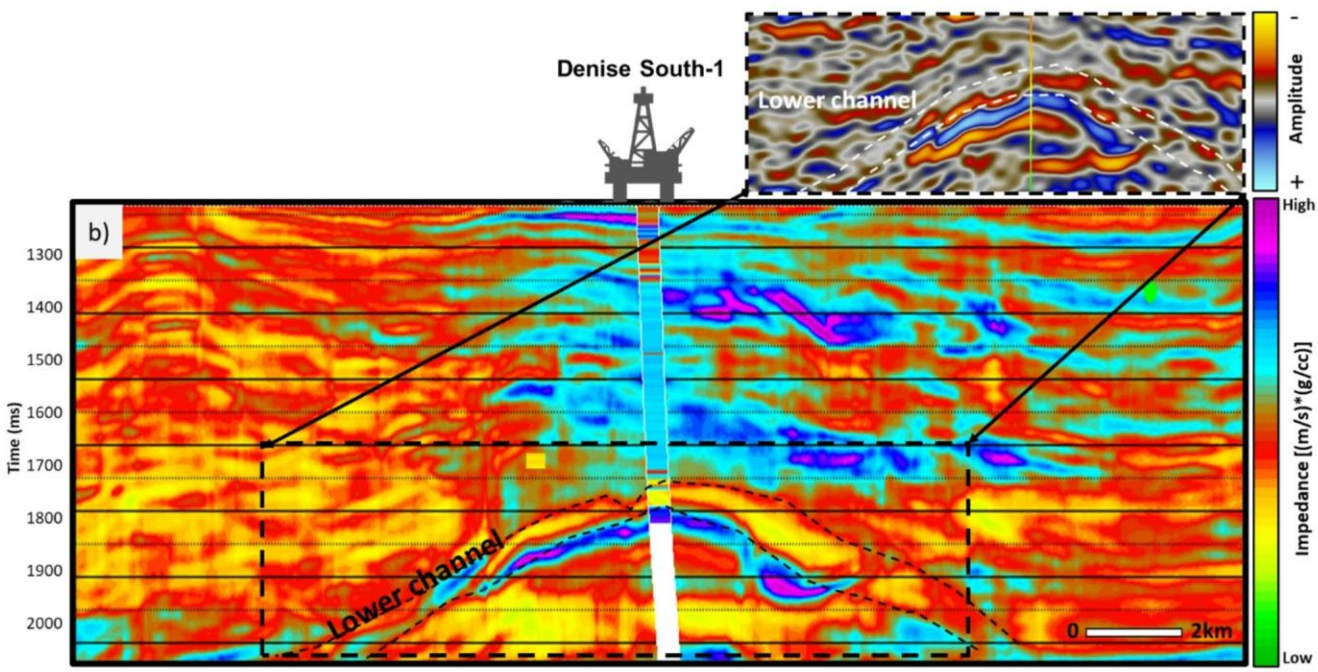

Fig. 12 Inverted P-impedance sections at the Denise-1 **a** and Denise South-1 **b** well locations. The color-coded impedance sections highlight low-impedance anomalies associated with gas-bearing sands within the upper and lower channel intervals. The vertical colored strips represent well-log-derived P-impedance inserted into the seismic sections, demonstrating good agreement between inverted impedance and log data at the reservoir level

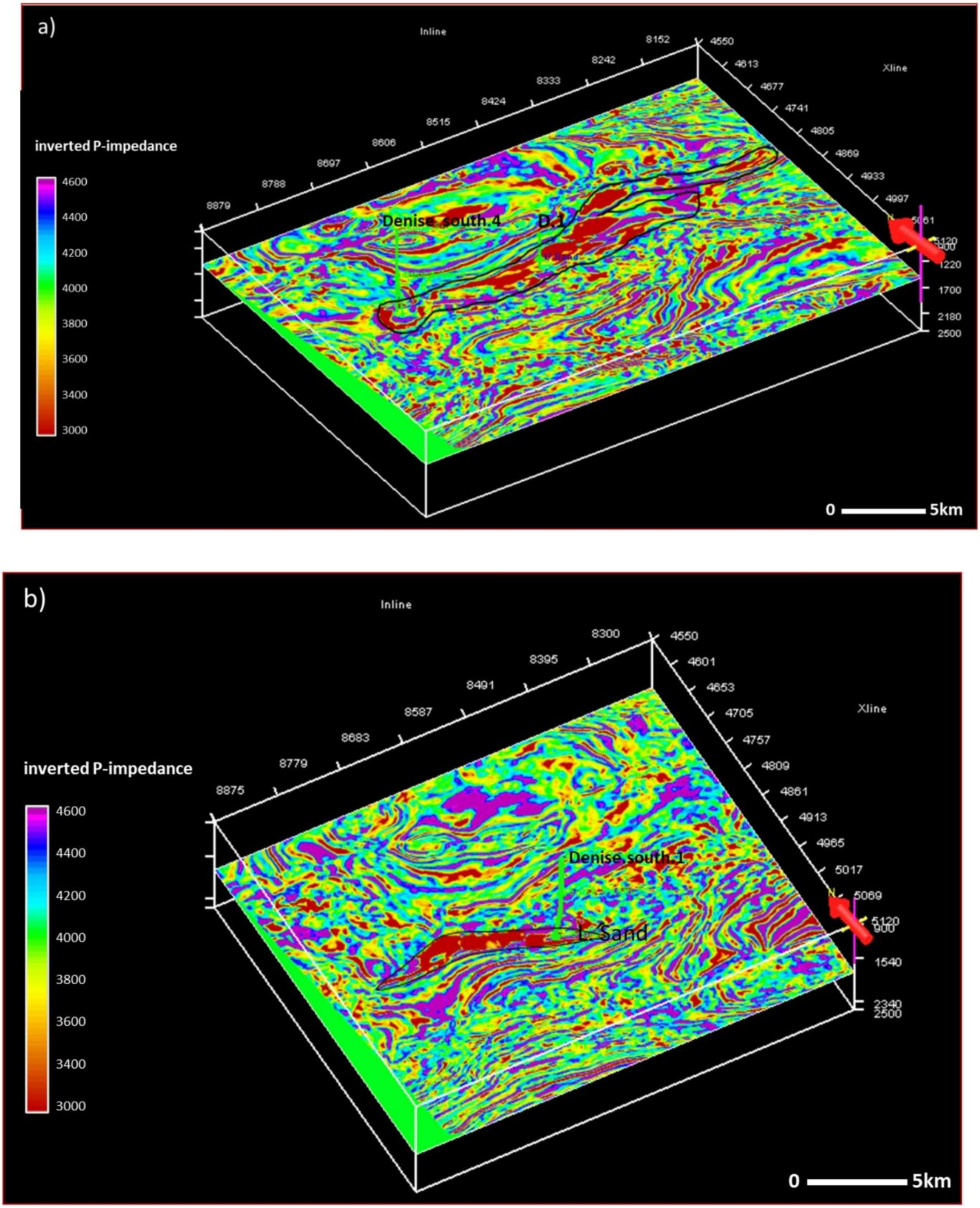

Fig. 13 Time slices of inverted P-impedance within the 1500–1800 ms interval illustrating **a** the upper channel and **b** the lower channel in the Denise Field. Low-impedance anomalies (warm colors) delineate channelized gas-bearing sands, while higher-impedance values correspond to surrounding shale-prone, water-saturated intervals

Table 6 Quantitative performance of the probabilistic neural network (PNN) in predicting clay volume (Vcl), effective porosity (PHIE), and water saturation (Sw) for the training dataset

Neural network		Vcl%	PHIE %	Sw %
Training	Correlation	0.90	0.87	0.87
	Error	0.046	0.044	0.16
validation	Correlation	0.74	0.64	0.53
	Error	0.22	0.066	0.25

volumes, which were subsequently validated against blind well data to ensure geological plausibility.

The final PNN models incorporated twelve optimized seismic attributes selected through stepwise multi-linear regression analysis based on their predictive contribution and their ability to reduce validation error. The selected attributes included acoustic impedance-derived attributes, integrated amplitude, amplitude envelope, instantaneous phase, instantaneous frequency, quadrature trace, second-derivative of instantaneous amplitude, sweetness, RMS amplitude, relative acoustic impedance, cosine of instantaneous phase, and variance. Attribute ranking and correlation analyses were performed iteratively during the regression stage to evaluate the relative contribution of each attribute to the prediction of clay volume, effective porosity, and water saturation. The ranking results indicated that AI-derived attributes, amplitude envelope, and integrated amplitude consistently showed the strongest correlations with reservoir-property variations, reflecting their sensitivity to lithology and fluid content in channel-sized reservoirs. In contrast, higher-order instantaneous and geometric attributes provided secondary but complementary contributions by enhancing subtle lateral heterogeneity and channel-boundary delineation. The stepwise selection procedure also minimized attribute redundancy and multi-collinearity, thereby improving model interpretability and prediction stability. A summary table listing the selected attributes and their relative ranking contributions has been added to the revised manuscript to further improve transparency and reproducibility.

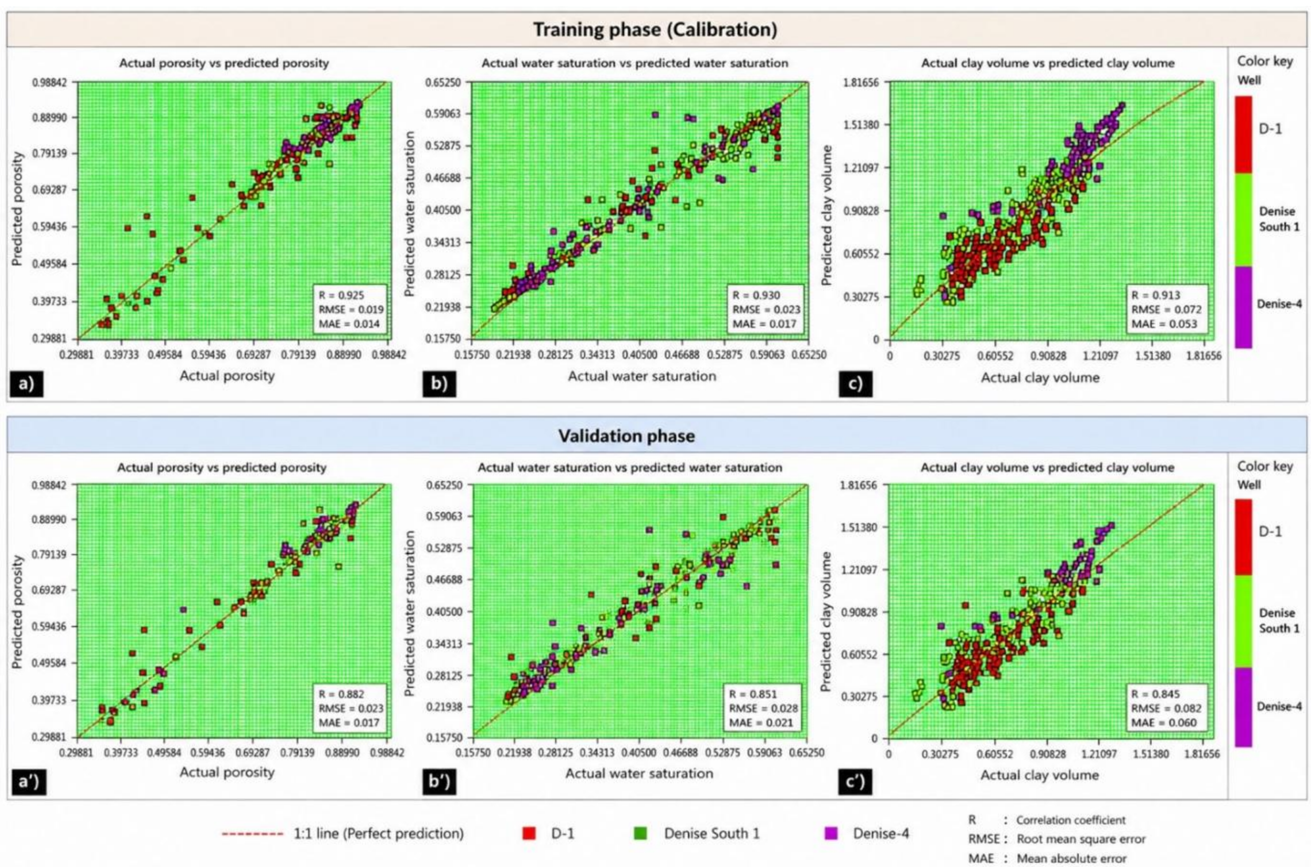

Fig. 14 Cross-plots comparing actual and predicted reservoir properties during the training **a**–**c** and validation **a′**–**c′** phases of the probabilistic neural network (PNN) model. Panels show effective porosity (PHIE), water saturation (Sw), and shale volume (VSh) for the three wells (Denise-1, Denise South-1, and Denise-4). Correlation coefficient (R), root mean square error (RMSE), and mean absolute error (MAE) are displayed to assess model performance and generalization capability

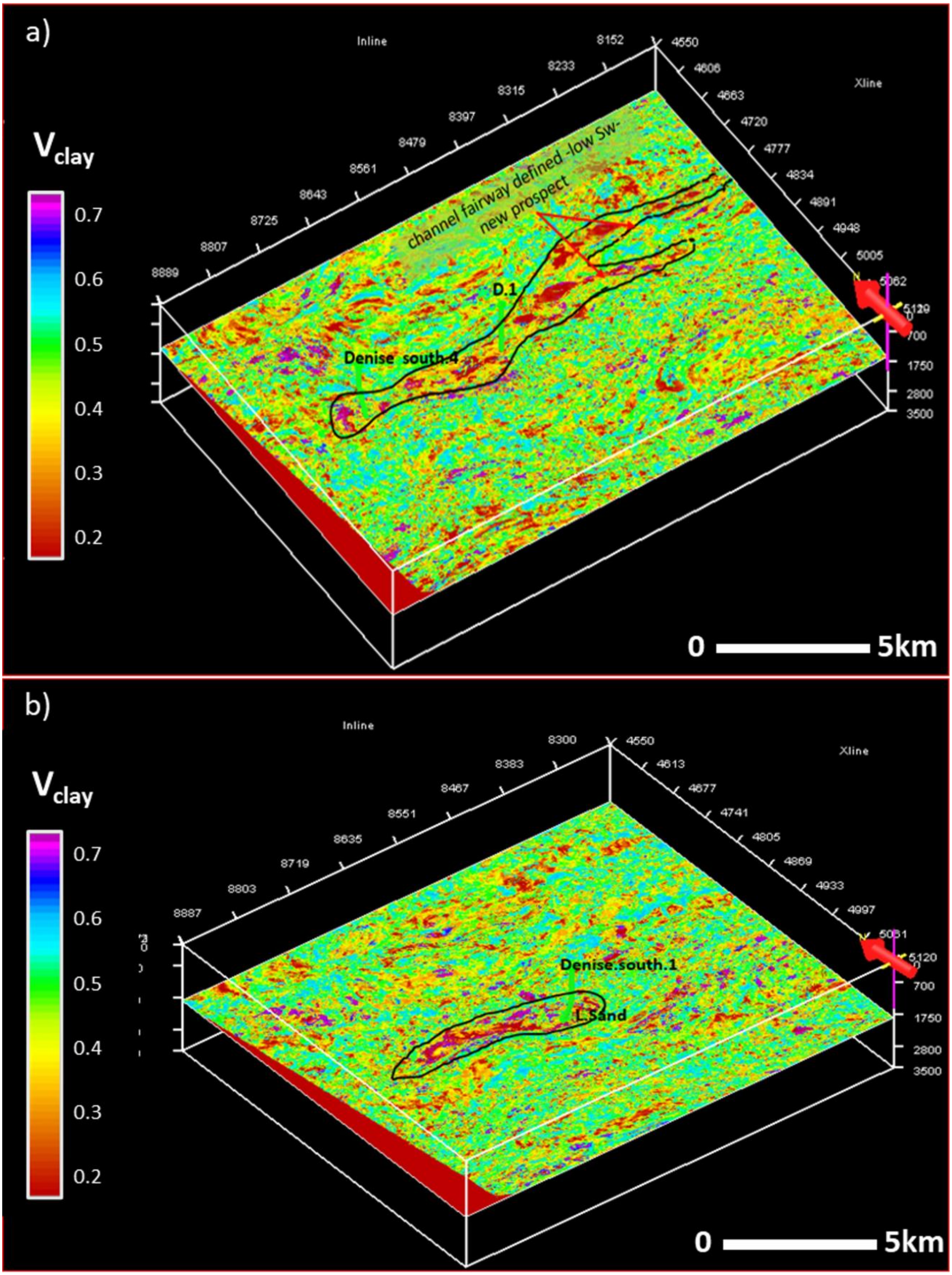

a)
Inline
8152
8233
8315
8397
8479
8561
8643
8725
8807
8889
Xline
4550
4606
4663
4720
4777
4834
4891
4948
5005
5062
700
1750
2800
3500
V_{clay}
0.7
0.6
0.5
0.4
0.3
0.2
channel fairway defined -low Sw-
new prospect
D.1
Denise south.4
0
5km
b)
Inline
8300
8383
8467
8551
8635
8719
8803
8887
Xline
4550
4613
4677
4741
4805
4869
4933
4997
5061
5120
700
1750
2800
3500
V_{clay}
0.7
0.6
0.5
0.4
0.3
0.2
Denise.south.1
L.Sand
0
5km

◀ **Fig. 15** Clay volume (Vcl) time-slice maps within the 1500–1800 ms interval for **a** the upper channel and **b** the lower channel in the Denise Field. The maps clearly distinguish lithological variations, with low clay volume highlighting sand-prone channel fairways. The upper-channel map shows a well-defined channel trend with reduced shale content, particularly toward the eastern sector, indicating improved reservoir quality

4 Results

4.1 Post-stack acoustic impedance inversion

The post-stack seismic inversion yielded a high-resolution P-wave acoustic impedance (AI) volume that is well-calibrated to the available well-log data. At the well locations, the inverted AI shows a strong agreement with log-derived impedance values, with correlation coefficients exceeding 90%, indicating a robust and reliable inversion outcome (Fig. 12). This close match confirms the effectiveness of the adopted model-based inversion workflow, including wavelet estimation, low-frequency model construction, and seismic-to-well calibration.

Away from direct well control, the inverted AI volume preserves laterally continuous and geologically consistent impedance trends across the study area. Clear impedance contrasts are observed, effectively delineating lithological boundaries within the reservoir interval. In particular, pronounced low-impedance anomalies are evident within both the upper and lower channel systems. In contrast, higher AI values are associated with surrounding shale-dominated intervals and water-saturated sands (Fig. 13).

The spatial distribution of the low-AI anomalies highlights the geometry and extent of the channelized sand bodies. Laterally continuous low-impedance zones are interpreted as well-connected, gas-charged reservoirs, indicating favorable connectivity and enhanced hydrocarbon accumulation potential. Conversely, areas with elevated AI values likely represent tighter lithologies or water-bearing intervals that may act as baffles or barriers to fluid flow.

4.2 Probabilistic neural network (PNN) predictions

The probabilistic neural network (PNN) successfully predicted key petrophysical properties—clay volume (Vcl), effective porosity (ϕ), and water saturation (Sw)—from the optimized seismic attribute volumes selected through step-wise regression (Table 6). The resulting prediction volumes clearly capture reservoir heterogeneity and fluid distribution patterns critical to reservoir evaluation and development planning. Cross-correlation between the PNN-predicted properties and the corresponding well-log-derived values consistently shows strong agreement across all wells, confirming the robustness of the PNN application.

The PNN-derived clay volume predictions show an excellent match with well-log data. Figure 14 illustrates cross-plots of measured clay volume from logs (x-axis) versus PNN-predicted values (y-axis) for all wells, yielding an average correlation coefficient of approximately 0.98. This high correlation indicates that the selected seismic attributes effectively capture lithological variations within the reservoir interval. The predicted lithology maps (Fig. 15) clearly delineate the upper and lower sand channel systems in the Denise area and are in close agreement with previous geological and seismic interpretations. The spatial distribution of low clay volume corresponds to sand-prone intervals identified in the wells, while higher clay volumes are associated with shale-dominated facies. The predicted lithology volumes show strong agreement with well-log observations.

Porosity prediction results further demonstrate the PNN model's strong performance. Cross-plots of original log-derived porosity versus predicted porosity values (Fig. 14b) show an average correlation coefficient of about 0.98, indicating excellent predictive accuracy. The 3D porosity volumes generated from the trained PNN (Fig. 16) highlight distinct high-porosity zones within both the upper and lower channel systems. Based on the applied color scale, porosity values range from 0 to 50%, with the highest porosity concentrations occurring within the channel axes, particularly around the drilled wells in the exploited zones. These high-porosity intervals are most prominent within the 1515–1800 ms time window. The lateral continuity of elevated porosity values suggests a well-developed, later-ally extensive reservoir quality across the channel complexes, supporting favorable reservoir connectivity.

Water saturation predictions also show a strong correspondence with well data. Figure 10c presents cross-plots of measured water saturation from logs versus PNN-predicted values, yielding an average correlation coefficient of approximately 0.87. The predicted water saturation volumes for the upper and lower channels (Fig. 17) reveal Sw values ranging from 20 to 100%, with significantly lower saturation values (20–45%) concentrated within the channel bodies. At the well locations, water saturation values are generally less than 25%, indicating gas-charged reservoir intervals. Importantly, the low Sw zones coincide spatially with the low-acoustic-impedance anomalies identified by seismic inversion, providing independent validation of the PNN predictions. This consistency between impedance-derived gas indicators and PNN-based saturation estimates strongly supports the interpretation of producible

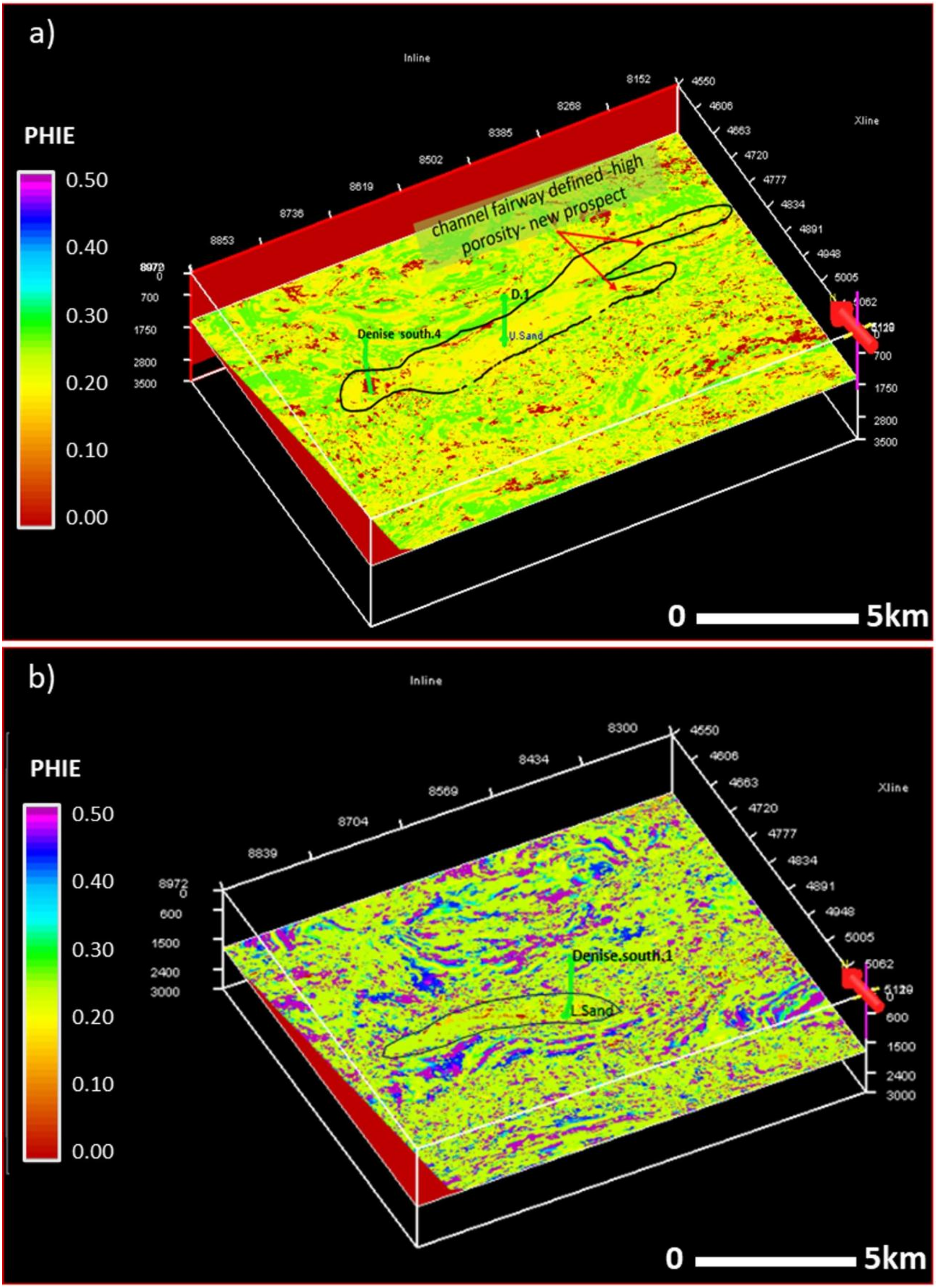

a)
Inline
PHIE
0.50
0.40
0.30
0.20
0.10
0.00
8152
8268
8385
8502
8619
8736
8853
Xline
4550
4606
4663
4720
4777
4834
4891
4948
5005
5062
channel fairway defined -high porosity- new prospect
D.1
U.Sand
Denise south.4
0
700
1750
2800
3500
0
5km
b)
Inline
PHIE
0.50
0.40
0.30
0.20
0.10
0.00
8300
8434
8569
8704
8839
8972
Xline
4550
4606
4663
4720
4777
4834
4891
4948
5005
5062
Denise.south.1
L.Sand
0
600
1500
2400
3000
0
5km

Fig. 16 Effective porosity time-slice maps within the 1500–1800 ms interval for **a** the upper channel and **b** the lower channel in the Denise Field. The maps clearly delineate lithological variations, with high-porosity values outlining sand-prone channel fairways. The upper-channel map highlights a well-defined fairway toward the eastern sector, interpreted as a high-quality reservoir zone

hydrocarbon-bearing sands within the upper and lower channel systems.

4.3 Integrated seismic–petrophysical interpretation

The integration of seismic-derived acoustic impedance (AI) volumes with PNN-predicted petrophysical properties provides a coherent and physically consistent framework for evaluating reservoir quality and hydrocarbon potential in the study area. A comparative analysis of the AI, effective porosity (ϕ), and water saturation (Sw) volumes reveals systematic spatial relationships that enhance confidence in the reservoir interpretation.

First, the western segment of the upper channel is characterized by consistently low AI values that spatially coincide with low clay volume, high porosity, and low water saturation. This combination of attributes indicates a clean, well-sorted sand body with favorable reservoir quality and effective hydrocarbon charge. The strong lateral continuity of these low-AI, high-ϕ, and low-Sw zones suggests good reservoir connectivity and supports the interpretation of a laterally extensive, gas-bearing channel complex.

Second, a gradual degradation in reservoir quality is observed toward the channel margins. These areas are characterized by increased shale content (higher Vcl), reduced porosity, locally elevated water saturation, and higher acoustic impedance. Such trends are consistent with depositional facies transitions from channel-axis sands to marginal or overbank deposits, as well as possible diagenetic effects that may have reduced pore space and permeability. These marginal zones likely act as baffles to fluid flow, contributing to heterogeneity within the internal reservoir.

5 Discussion

5.1 Seismic–petrophysical consistency and reservoir behavior

The integrated interpretation of post-stack acoustic impedance (AI) inversion and probabilistic neural network (PNN)–derived petrophysical properties provides a consistent and physically meaningful description of reservoir behavior in the Temsah area. A strong spatial association between low AI values, high effective porosity (ϕ), and low water saturation (Sw) is evident within the upper and lower channel systems (Figs. 9, 10, 11, 12, 13, 14, 15, 16 and 17). This relationship is consistent with established rock-physics concepts, whereby gas-charged sands exhibit reduced acoustic impedance due to lower bulk density and elastic moduli than water-bearing sands and shale-prone intervals (Russell 1988; Bertello et al. 1996a, 1996b; Smith and Treitel 2010). These impedance patterns are consistent with established rock-physics behavior, in which gas-bearing sands exhibit reduced acoustic impedance due to fluid-sub-situation effects and lower bulk density.

The high correlations between PNN-predicted properties and well-log measurements (Fig. 14) confirm the robustness of the machine-learning workflow and indicate that the selected seismic attributes effectively capture lithological and fluid-related variations. The lateral continuity of low-AI, high-ϕ, and low-Sw zones along the channel axes suggests well-connected reservoir bodies with limited internal compartmentalization. In contrast, increasing clay volume and decreasing porosity toward the channel margins reflect depositional facies changes and possible diagenetic effects that may locally affect permeability and fluid-flow efficiency.

The PNN-derived reservoir-property sections reveal clear spatial variations in shale volume (VSh), water saturation (Sw), and effective porosity (PHIE) within the studied channel systems (Fig. 18). The upper-channel interval at the Denise-1 well is characterized by relatively low VSh and Sw values associated with elevated PHIE, indicating the presence of clean, porous reservoir sands with favor-able hydrocarbon potential. Similarly, the lower-channel interval penetrated by the Denise South-1 well exhibits a distinct reduction in shale content and water saturation, accompanied by enhanced porosity, confirming its reservoir quality. The close correspondence between the predicted reservoir-property distributions and the interpreted channel geometries demonstrates the PNN model's ability to capture lateral and vertical heterogeneities within the reservoir. These results support the interpretation that the channel complexes represent the most prospective hydro-carbon-bearing zones within the Denise Field.

Although the predicted petrophysical volumes show strong agreement with well-log observations, uncertainty associated with seismic-based property prediction must be considered, particularly in areas distant from well control. To evaluate prediction reliability, validation errors, and root mean square error (RMSE) distributions were continuously monitored during the PNN training and blind-testing

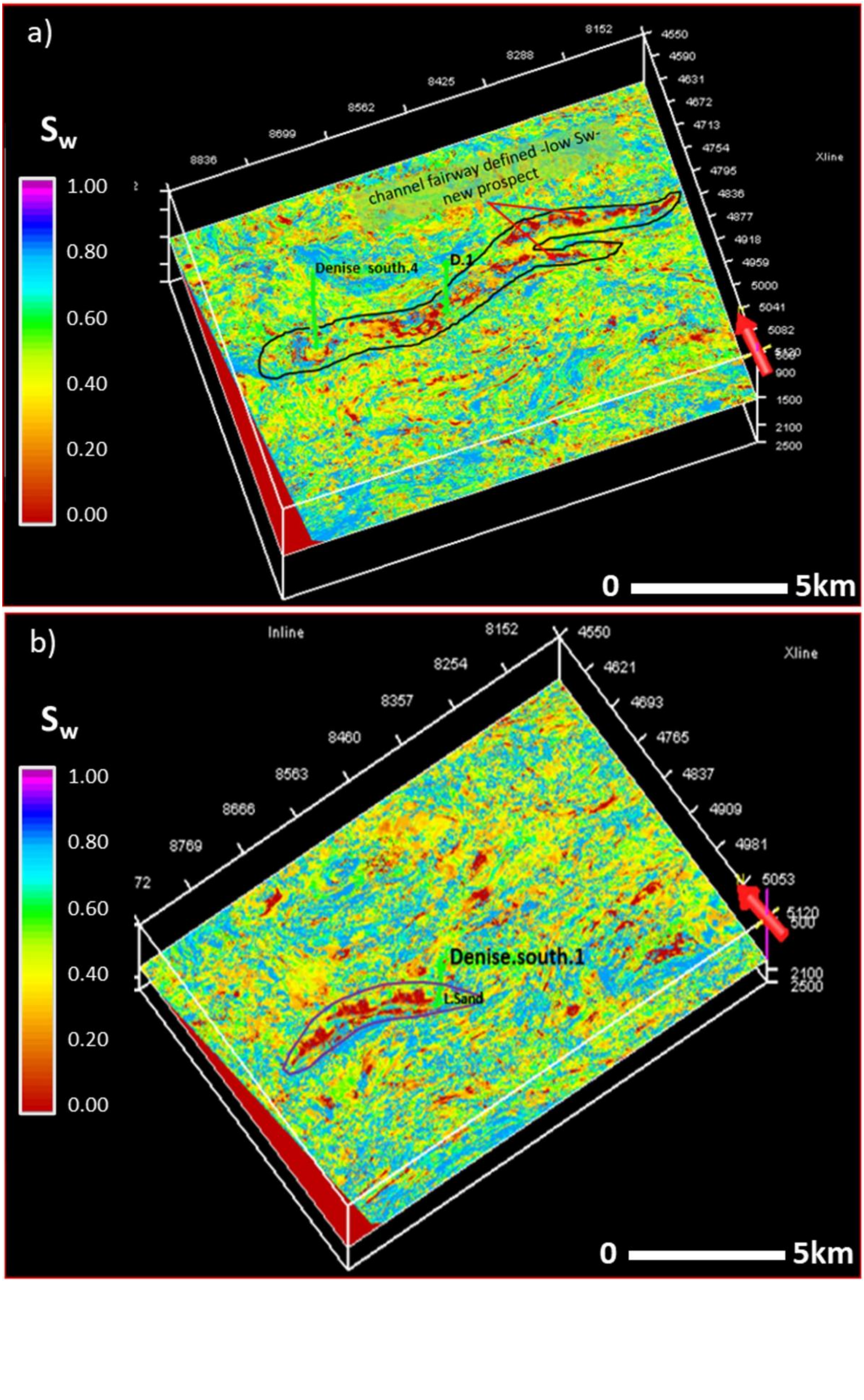
a)
S_w
1.00
0.80
0.60
0.40
0.20
0.00
8152
8288
8425
8562
8699
8836
4550
4590
4631
4672
4713
4754
4795
4836
4877
4918
4959
5000
5041
5082
5120
900
1500
2100
2500
Xline
channel fairway defined -low Sw-
new prospect
Denise south.4
D.1
0
5km
b)
Inline
Xline
S_w
1.00
0.80
0.60
0.40
0.20
0.00
8152
8254
8357
8460
8563
8666
8769
4550
4621
4693
4765
4837
4909
4981
5053
5120
500
2100
2500
Denise.south.1
L.Sand
0
5km

Fig. 17 Water saturation (Sw) time-slice maps within the 1500–1800 ms interval for **a** the upper channel and **b** the lower channel in the Denise Field. Low-Sw zones delineate sand-prone channel fairways, with the upper-channel map highlighting a well-defined fairway toward the eastern sector characterized by reduced water saturation, indicative of gas-charged reservoir intervals

stages. The lowest prediction uncertainties were observed in the vicinity of the calibrated wells and along laterally continuous channel fairways, where seismic responses and inversion-derived impedance trends exhibit strong consistency. In contrast, uncertainty increases toward channel margins and structurally complex areas, which are characterized by weaker seismic continuity and reduced calibration control. Sensitivity analysis further demonstrated that the prediction results are most strongly influenced by AI-derived attributes and amplitude-related seismic responses, whereas secondary attributes primarily enhance local heterogeneity. Although the present study focuses primarily on deterministic reservoir characterization, the observed spatial variation in prediction errors provides an important qualitative measure of model confidence and the reliability of interpretation. Future work should incorporate fully probabilistic uncertainty-quantification workflows, including spatial RMSE maps, prediction intervals, and ensemble learning approaches, to further constrain reservoir-property uncertainty beyond well control.

5.2 Development significance and risk considerations

From a development perspective, the integrated results provide clear guidance for prioritizing reservoir targets. The western segment of the upper channel emerges as the most attractive zone, characterized by low shale content, high porosity, and low water saturation (Figs. 9a and 13a). These attributes indicate a high-quality, gas-charged reservoir with favorable lateral connectivity, making it a prime candidate for infill drilling and production optimization.

The interpretation of low acoustic impedance (AI) anomalies as gas-bearing sands is supported by quantitative rock-physics relationships observed in the available well-log data (Fig. 19). Cross-plot analysis between acoustic impedance, effective porosity, and water saturation demonstrates that intervals characterized by low AI values consistently correspond to high-porosity and low-water-saturation reservoir zones within the upper and lower channel systems. In contrast, shale-dominated and water-bearing intervals exhibit relatively higher AI values due to increased bulk density and elastic stiffness. These trends are consistent with established rock-physics principles, in which gas charging reduces P-wave velocity and bulk density, thereby lowering acoustic impedance. Furthermore, the spatial coincidence between low-AI anomalies and PNN-predicted low-water-saturation zones provides additional independent support for the interpretation of gas-bearing channel sands. To improve the robustness of this interpretation, cross-plots between inverted AI and well-log-derived reservoir properties have been added to the revised manuscript, highlighting the quantitative relationship between elastic properties and reservoir fluid distribution.

Despite the strengths of the integrated inversion–PNN approach, uncertainty management remains critical (Smith and Treitel 2010; Zheng et al. 2014). While seismic inversion and neural-network predictions significantly reduce interpretation ambiguity, their reliability is closely tied to the quality and spatial distribution of well control. Areas with sparse log data inherently carry higher uncertainty, underscoring the importance of continued calibration as new wells become available. Integrating additional data types, such as pressure measurements or production data, would further constrain predictions of reservoir performance and reduce development risk.

5.3 Context within regional studies and added value of the workflow

The results of this study are consistent with previous regional investigations that identify channelized reservoirs as the primary hydrocarbon-bearing elements within the Temsah Formation and the offshore Nile Delta province (Abd El Aal et al. 1994; Kirschbaum et al. 2010; Dolson et al. 2019). However, the present work extends earlier studies by combining post-stack AI inversion with probabilistic neural networks, yielding enhanced spatial resolution and a more quantitative characterization of reservoir properties.

Compared with conventional seismic attribute interpretation alone, the proposed workflow enables direct prediction of clay volume, porosity, and water saturation, resulting in a more detailed and geologically consistent reservoir model. The demonstrated agreement between seis-mic indicators and petrophysical predictions highlights the added value of integrating deterministic and data-driven techniques. Overall, this approach improves reservoir understanding, enhances confidence in identifying producible hydrocarbon zones, and helps reduce exploration and development uncertainty.

5.4 Methodological implications and limitations of the PNN workflow

Although probabilistic neural networks (PNNs) represent an established machine-learning technique in seismic

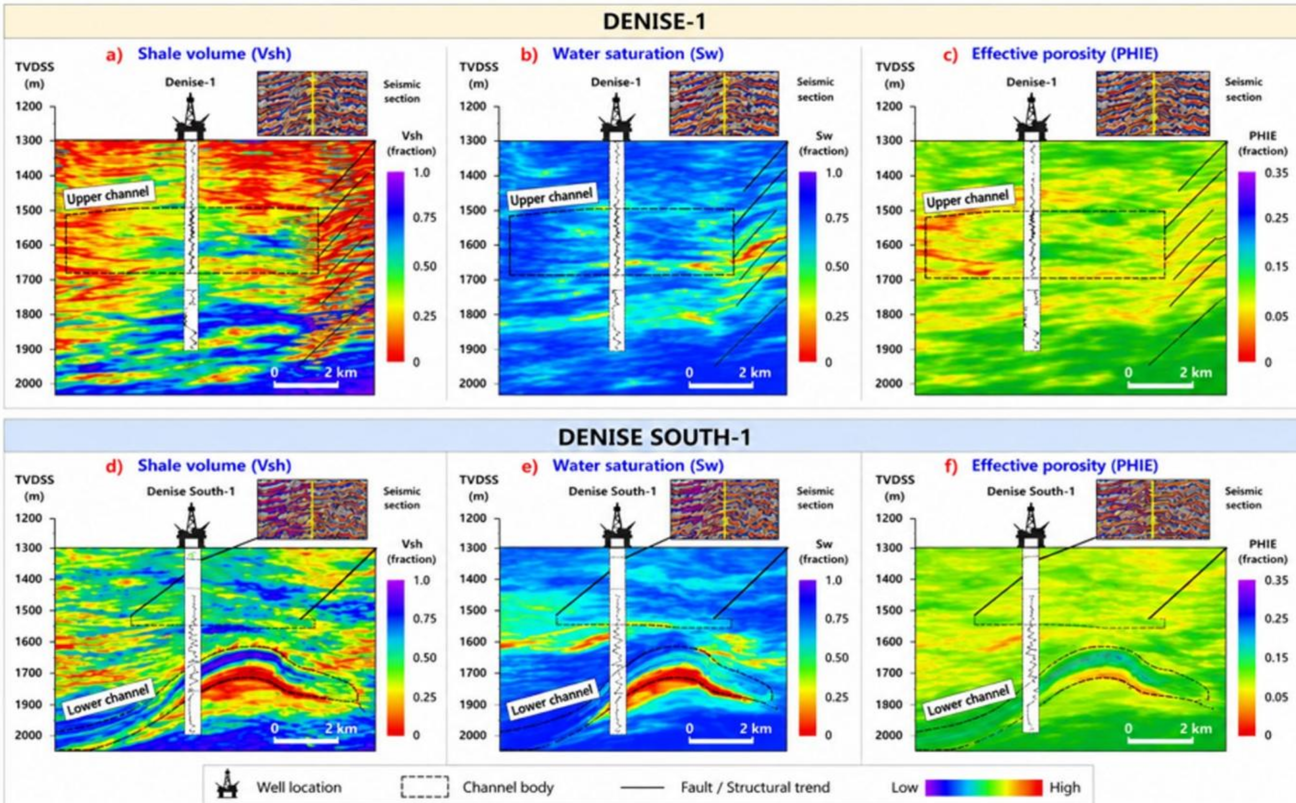

Fig. 18 Cross-sections of shale volume (VSh), water saturation (Sw), and effective porosity (PHIE) predicted from the probabilistic neural network (PNN) model along two representative seismic profiles crossing the Denise-1 **a**–**c** and Denise South-1 **d**–**f** wells. The sections illustrate the spatial distribution of reservoir properties within the upper and lower channel systems. Low shale volume, low water saturation, and high effective porosity coincide with the channel reservoirs, indicating favorable hydrocarbon-bearing intervals

reservoir characterization, the present study emphasizes the integration of PNN modeling with high-resolution post-stack acoustic impedance inversion within a geologically complex offshore Nile Delta setting, where sparse well control, strong lateral facies variability, and channelized depositional architectures pose significant interpretation challenges. The methodological contribution of this work does not primarily reside in introducing a new machine-learning algorithm, but rather in developing a robust integrated inversion–machine-learning workflow that combines deterministic elastic-property constraints with data-driven petrophysical prediction to improve reservoir delineation and reduce interpretation uncertainty. Recent machine-learning methods such as Random Forest (RF), Extreme Gradient Boosting (XGBoost), and deep neural networks (DNNs) have demonstrated promising performance in seis-mic-based reservoir-property prediction; however, these approaches generally require substantially larger and more diverse training datasets to ensure stable generalization and avoid overfitting. In the Denise Field, the limited number of available wells (three calibrated wells) and the relatively small training dataset favored the adoption of the PNN approach because of its robustness to small-to-moderate datasets, rapid convergence, and reduced sensitivity to initialization parameters. Furthermore, PNN models provide stable predictions while preserving geological consistency with inversion-derived acoustic impedance trends. Nevertheless, the authors acknowledge that future studies should include systematic benchmarking against advanced ensemble learning and deep learning algorithms, particularly as larger, higher-quality databases and broader training datasets become available. Such a comparative analysis would provide additional insight into the relative predictive performance, uncertainty behavior, and computational efficiency of different machine-learning approaches for off-shore Nile Delta reservoir characterization.

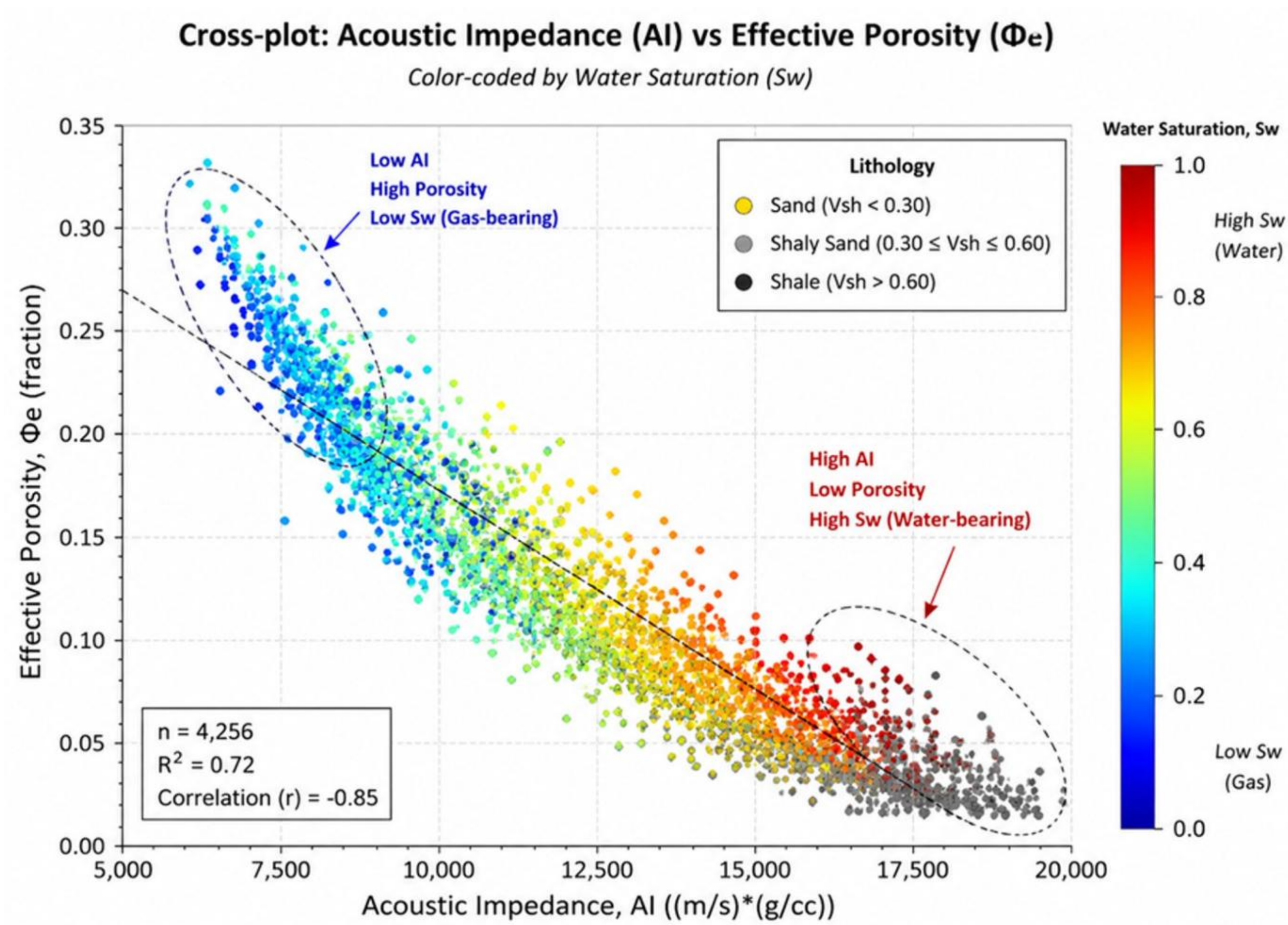

Fig. 19 Cross-plot of acoustic impedance (AI) versus effective porosity (Φe) for the Denise Field reservoirs. The plot shows a strong inverse relationship: low AI values correspond to high porosity and low water saturation in gas-bearing sands, whereas high AI values are associated with shale-prone and water-bearing intervals

6 Conclusions

This study presents an integrated seismic–petrophysical workflow for reservoir characterization in the Denise Field, offshore Nile Delta, that combines post-stack acoustic impedance (AI) inversion with probabilistic neural network (PNN)– based property prediction.

The model-based AI inversion produced a high-resolution impedance volume that is well calibrated to well-log data and preserves geologically consistent impedance trends away from well control. Low-impedance anomalies clearly delineate the upper and lower channel systems and are interpreted as gas-bearing sands. In contrast, higher AI values correspond to shale-rich intervals and water-saturated sands.

The application of PNN modeling, trained using step-wise-optimized seismic attributes, successfully predicted key petrophysical properties, including clay volume (Vcl), effective porosity (ϕ), and water saturation (Sw). Strong correlations between predicted and well-derived properties confirm the robustness of the machine-learning approach. The resulting 3D property volumes reveal significant reservoir heterogeneity and clearly define channel geometries, highlighting laterally continuous, high-porosity and low-water-saturation zones along the channel axes.

Integration of AI inversion results with PNN-derived petrophysical volumes provides a coherent and physically consistent interpretation of reservoir quality and fluid distribution. The western segment of the upper channel is identified as the most prospective reservoir zone, characterized by low shale content, high porosity, and low water saturation, indicating a well-connected gas-charged sand body with favorable development potential. In contrast, reduced reservoir quality toward channel margins reflects facies transitions and possible diagenetic effects that may locally influence fluid flow.

Overall, this work demonstrates that the combined use of post-stack seismic inversion and probabilistic neural networks significantly enhances reservoir characterization in complex clastic systems. The integrated workflow reduces interpretation uncertainty, improves prediction of reservoir properties away from well control, and provides a reliable basis for identifying producible hydrocarbon zones.

Future studies should focus on incorporating additional well data, rock-physics modeling, and pre-stack seismic inversion to further refine elastic–petrophysical relationships and improve confidence in reservoir development and optimization strategies.

Acknowledgements The authors sincerely thank the Egyptian General Petroleum Corporation (EGPC) for supplying the seismic and well-log datasets and for authorizing the publication of this work. The authors would like to express their gratitude to the Ongoing Research Funding Program (ORF-2026-781) at King Saud University, Riyadh, Saudi Arabia, for its financial support.

References

Abd El Aal A, Roger J, Price J, Vaitl D, Shrallow J (1994) Tectonic evaluation of the Nile Delta and its impact on sedimentation and hydrocarbon potential. In Proceedings of the 12th Exploration and Production Conference. Cairo: Egyptian General Petroleum Corporation (EGPC): 19–34

Abdel-Fattah MI, Slatt RM (2013) Sequence stratigraphic controls on reservoir characterization and architecture: case study of the Messinian Abu Madi incised-valley fill, Egypt, Central European. J Geosci 5(4):497–507

Abdel-Fattah MI, Sen S, Abuzied SM, Abioui M, Radwan AE, Benssaou M (2022) Facies analysis and petrophysical investigation of the Late Miocene Abu Madi sandstone gas reservoirs, offshore Baltim East Field, Nile Delta, Egypt. Mar Pet Geol 137:105501. https://doi.org/10.1016/j.marpetgeo.2021.105501

Abdel-Fattah MI, Hamdan HA, Sarhan MA (2023) Hydrocarbon potential and reservoir characteristics of incised-valley transgressive sandstones: a case study from the Messinian gas reservoirs, Nile Delta Basin, Egypt. J Afr Earth Sc 207:105073. https ://doi.org/10.1016/j.jafrearsci.2023.105073

Abdel-Fattah MI, Hamdan HA, Mahdi AQ, Abd-Allah ZM, Hammouri NA, Abuzied SM (2025) Integrated geological, petrophysical, geochemical and geomechanical evaluation of shale gas potential in the Khatatba Formation. Western Desert, Egypt, Petroleum Research

Abdel-Rahman AS, Reda M, Abdel-Hafez NA, Mahmoud MAK (2025) Source rock evaluation and basin modeling of Pliocene formations in Sapphire gas field, offshore Nile Delta. Mediterranean Geoscience Reviews 7(4):1227–1251. https://doi.org/10 .1007/s42990-025-00185-3

Al-Sharhan AS, Salah MG (1997) Geology and hydrocarbon habitat in the Nile Delta. J Pet Geol 20(3):313–332

Amir HS, Fathy M, Reda M, Mostafa T (2025a) Integrated core-log petrophysical evaluation of the Sarir Formation reservoir units, southeastern Sirte Basin, Libya, Journal of Umm Al-Qura University for Applied Sciences: 1–20. https://doi.org/10.1007/s43994-025-00295-6

Amir HS, Omar AE, Abdel-Fattah MI, Amir MA, Al-Hashim MH, Bendawi AS, Reda M (2025b) Toward successful drilling operations through geomechanical modelling and wellbore stability analysis: a case study of the Ouan Kasa Reservoir in the Gha-dames Basin, Libya. Pet Geosci. https://doi.org/10.1144/petgeo 2024-069

Amir MA, Amir HS, Abdel-Fattah MI, Elsteil MO, Mogren S, Ibrahim E, Reda M (2025c) New approach to reduce the uncertainty level of the shear wave velocity prediction by utilizing ensemble model: a case study from Sirt Basin, Libya. Earth Sci Inf 18(3):463. https://doi.org/10.1007/s12145-025-01962-2

Anwar S, El Kadi HH, Hosny A, Reda M, Mostafa T (2025) Identifying gas bearing sand using simultaneous pre-stack seismic inversion method: case study of the Simian field, Offshore Nile Delta, Egypt. J Petroleum Explor Prod Technol 15(4):1–16. https://doi.org/10.1007/s13202-025-01971-3

Ayyad MH, Darwish M (1996) Syrian Arc structures: a unifying model of inverted basins and hydrocarbon occurrences in North Egypt, in Proceedings of the 13th EGPC Exploration and Production Conference. Cairo: 40–60

Badalini G, Blendinger W, Kabbej A, Le Roy P, Raef A (2020) Petroleum systems of the Nile Delta Basin. AAPG Bull 104(7):1409–1443

Bertello F, Barsoum K, Dalla S, Guessarian S (1996a) Temsah discovery: a giant gas field in a deep-sea turbidite environment, in Proceedings of the 13th EGPC Exploration and Production Conference. Cairo: 165–180

Bertello F, Rahman H, Bocca P, Cegani D, Ronchitelli G (1996b) Temsah 3D reprocessing: revealing seismic pitfalls in the Tau-P domain, in Proceedings of the 13th EGPC Exploration and Production Conference. Cairo: 99–107

Court J (2009) Simultaneous inversion of pre-stack seismic data for quantitative interpretation: Simian and Sienna fields, Egypt. MSc Thesis. University of Leeds

Doherty M, Jamieson G, Kilanyi T, Trayner P (1988) Geology and seismic stratigraphy of the offshore Nile Delta, Egypt, in Proceedings of the 9th EGPC Exploration and Production Conference. Cairo: 408–425

Dolson J (2019) The petroleum geology of Egypt and history of exploration. In: Hamimi Z et al (eds) The Geology of Egypt. Springer, Cham, pp 1–49. https://doi.org/10.1007/978-3-030-15265-9_16

Elgendy NH, Reda M, Elmashaly MM, Raef A, Al-Hashim MH, Barakat MK (2024) Three-dimensional reservoir modeling of the Pliocene reservoir based on seismic data advances for new prospect assessment. Mar Georesour Geotechnol 1–18. https://doi.org/10.1080/1064119X.2024.2400689

Fathy M, Reda M, Abdel-Fattah MI, Raef A, Al-Hashim MH (2025a) Seismic and petrophysical characterization of the Sequoia Pliocene channel reservoirs: insights into hydrocarbon potential in

the West Delta Deep Marine, Egypt. https://doi.org/10.1144/petgeo2024-070., Petroleum Geoscience
Fathy M, Reda M, Abdel-Fattah MI, Sadoun M, Raef A, Al-Kahtany K, Farouk S (2025b) Assessment of late miocene reservoirs: geophysical and petrophysical perspectives on unconventional gas in the Nidoco Field, Nile Delta, Egypt, Geological Journal. https://doi.org/10.1002/gj.5245
Fathy M, Reda M, Abdel-Fattah MI, Sadoun M, Raef A, Al-Kahtany K, Farouk S (2026) Assessment of late miocene reservoirs: geophysical and petrophysical perspectives on unconventional gas in the Nidoco Field, Nile Delta. Egypt Geol J 61(2):509–528
Hampson DP, Schuelke JS, Quirin JA (2001) Use of multiattribute transforms to predict log properties from seismic data. Geophysics 66(1):220–236. https://doi.org/10.1190/1.1444899
Harwood C, Hodgson N, Ayyad M (1998) Sequence stratigraphic applications in Plio-Pleistocene exploration, Nile Delta, in EGPC Exploration and Production Conference Proceedings. Cairo: 1–13
Kirschbaum MA, Schenk CJ, Charpentier RR, Klett TR, Brownfield ME, Pitman JK, Cook TA, Tennyson ME (2010) Assessment of undiscovered oil and gas resources of the Nile Delta Basin Province, Eastern Mediterranean. US Geological Survey, pp 2010–3027
Latimer RB, Davidson R, Van Riel P (2000) An interpreters guide to understanding and working with seismic-derived acoustic impedance data. Lead Edge 19(3):242–256
Leisi A, Saberi MR (2023) Petrophysical parameters estimation of a reservoir using integration of wells and seismic data: a sandstone case study. Earth Sci Inf 16(1):637–652. https://doi.org/10.1007/s12145-022-00902-8
Leisi A, Shad Manaman N (2024a) Three-dimensional shear wave velocity prediction by integrating post-stack seismic attributes and well logs: application on Asmari formation in Iran. J Petroleum Explor Prod Technol 14(8):2399–2411. https://doi.org/10.1007/s13202-024-01832-5
Leisi A, Shad Manaman N (2025a) Geomechanical characterization of Asmari formation in the Dezful Embayment via simultaneous inversion and extended elastic impedance techniques, SW Iran, Earth Science Informatics, 18(4): 337. https://doi.org/10.1007/s12145-025-01853-6
Leisi A, Shad Manaman N (2025b) Seismic and geomechanical characterization of Asmari formation using well logs and simultaneous inversion in an Iranian oil field. Sci Rep 15(1):11276. https://doi.org/10.1038/s41598-025-95796-z
Leisi A, Aftab S, Manaman NS (2024b) Poro-acoustic impedance (PAI) as a new and robust seismic inversion attribute for porosity prediction and reservoir characterization. J Appl Geophys 223:105351. https://doi.org/10.1016/j.jappgeo.2024.105351
Leisi A, Aftab S, Manaman NS, Kadkhodaie A (2025) Prediction of bitumen distribution using seismic data inversion: application on the Kangan Formation, Persian Gulf Basin. Pet Sci Technol 1–21. https://doi.org/10.1080/10916466.2025.2537252
Leisi A, Kadkhodaie A, Kadkhodaie R (2026a) Integrated reservoir quality index (IRQI): a novel approach for reservoir quality assessment. Sci Rep 16:10596. https://doi.org/10.1038/s41598-026-46154-0
Leisi A, Khojasteh ER, Manaman NS (2026b) Integrated neural network–geostatistical modeling for data-driven estimation of shear wave velocity from conventional well logs: a case study from an Iranian oil reservoir. Results Eng 29:108855. https://doi.org/10.1016/j.rineng.2025.108855
Mascle G, Mascle J (2019) The Messinian salinity legacy: 50 years later. Mediterranean Geoscience Reviews 1:5–15. https://doi.org/10.1007/s42990-019-0002-5
Metwally AM, Mabrouk WM, Mahmoud AI, Eid AM, Amer M, Noureldin AM (2023) Formation evaluation of Abu Madi reservoirs, Baltim gas field. Nile Delta Sci Rep 13:19139. https://doi.org/10.1038/s41598-023-46239-4
Negm AM (2018) Reservoir characterization using seismic attributes and well logs, offshore Temsah Field, Nile Delta, Egypt. Ann Geol Surv Egypt 35:139–151
Negm AM, Abdel-Fattah MI, Al-Hashim MH, Reda M (2025) Seismic attribute integration and neural network analysis for quantitative reservoir characterization: a case study from the Offshore Nile Delta, Egypt. https://doi.org/10.1016/j.ptlrs.2025.09.004., P etroleum Research
Orwig ER (1982) Tectonic framework of North Egypt and the Eastern Mediterranean. In Proceedings of the 6th EGPC Exploration Seminar. Cairo: 20
Othman AAA, Fathy M, Negm AM (2018) Identification of channel geometries using seismic attributes and spectral decomposition, Temsah Field, offshore Nile Delta. NRIAG J Astron Geophys 7(1):52–61. https://doi.org/10.1016/j.nrjag.2018.01.005
Radwan MS, Gobashy MM, Dahroug S, Raslan S (2024) Exploration opportunities in East Mediterranean through Egypt's digital platform: a review. Mediterranean Geoscience Reviews 6(2):177–196. https://doi.org/10.1007/s42990-024-00124-8
Raef A, Jallow M, Cimino V, Hagood W, Reda M, Abd El-Moghny MW, Totten M (2025) Seismic attributes, sedimentary petrography, and ultrasonic laboratory measurements in enhanced reservoir characterization: the thin Viola carbonates, Kan-sas, USA. J Appl Geophys 105969. https://doi.org/10.1016/j. jappgeo.2025.105969
Reda M, El-Gendy NH, Raef A, Elmashaly MM, AlArifi N, Barakat MK (2024a) Advancing Neogene–Quaternary reservoir characterization in offshore Nile Delta, Egypt: high-resolution seismic insights and 3D modeling for new prospect identification. Environ Earth Sci 83(20):581. https://doi.org/10.1007/s12665-024-1 1846-1
Reda M, El-Gendy NH, Raef A, Elmashaly MM, AlArifi N, Barakat MK (2024b) High-resolution seismic interpretation and 3D modeling of Neogene–Quaternary reservoirs, offshore Nile Delta. Environ Earth Sci 83:581. https://doi.org/10.1007/s12665-024-1 1115-0
Reda M, Mostafa T, Abdel-Fattah MI, Amir HS, Amir MA, Raef A, Farouk S (2025b) Integrated petrophysical analysis, seismic interpretation, and 3D static reservoir modelling for rock typing and geomechanical characterisation of Cretaceous reservoirs in the Arcadia and Dorra oil fields, Western Desert, Egypt, Geological Journal. https://doi.org/10.1002/gj.70122
Reda M, El-Gendy NH, Abdel-Fattah MI, Elmashaly MM, Barakat MK (2025c) Enhancing reservoir characterization in the Temsah gas field through high-resolution seismic analysis and three-dimensional modeling. Sci Rep. https://doi.org/10.1038/s41598-025-22108-w
Rizzini A, Vezzani F, Cococcetta V, Milad G (1978) Stratigraphy and sedimentation of the Neogene–Quaternary section of the Nile Delta. Mar Geol 27:327–348. https://doi.org/10.1016/0025-3227(78)90038-5
Samuel A, Kneller B, Raslan S, Sharp A, Parsons C (2002) Prolific deep-marine slope channels of the Nile Delta. AAPG Bull 87(4):541–560
Sarhan MA (2022) Gas-generative potential of the post-Messinian megasequence, Nile Delta Basin. J Petroleum Explore Prod Technol 12(4):925–947
Sedki A, Abdelhady MAEM, Ahmed HE, Reda M (2025a) Petrophysical evaluation and 3D reservoir modeling in Qawasim Formation, El Basant Gas Field, Nile Delta, Egypt: insights from well-log analysis and 2D seismic data. Arab J Geosci 18(3):54. https://doi.org/10.1007/s12517-024-12174-1
Sedki A, Abdelhady MAEM, Ahmed HE, Reda M (2025b) Evaluation of the Qawasim formation through integration of available data

from El Basant wells, Nile Delta, Egypt. Arab J Geosci 18(6):1–23. https://doi.org/10.1007/s12517-025-12251-z

Selim E, Sarhan MA, Shalaby A (2024) Geophysical assessment of Pliocene gas-bearing sandstones, Kafr El-Sheikh Formation, offshore Nile Delta. Egyptian J Petroleum 33(3):6

Sestini G (1989) Nile Delta: depositional environments and geological history, geological society. Lond Special Publications 41(1):99–127

Shehata AA, Sarhan MA, Abdel-Fattah MI, Assal EM (2023) Sequence stratigraphic controls on the gas-reservoirs distribution and characterization along the Messinian Abu Madi incision, Nile Delta Basin. Mar Pet Geol 147:105988

Singh S, Kumar A, Mandal D (2016) Application of artificial neural networks in reservoir characterization. J Petroleum Explore Prod Technol 6:99–106

Smith T, Treitel S (2010) Self-organizing artificial neural nets for automatic anomaly identification. in SEG Tech Program Expanded Abstracts : 1403–1407

Todorov T, Hampson D, Russell B (1997) Sonic log prediction using seismic attributes. CREWES Res Rep 9:1–12

Zheng Y, Zhao T, Zhang G, Liu C (2014) Prediction of reservoir properties using seismic attributes and artificial neural network. J Appl Geophys 107:45–54